Precambrian Research 363 (2021) 106326

Contents lists available at ScienceDirect

Precambrian Research

journal homepage: www.elsevier.com/locate/precamres

Silver-gold and polymetallic mineralization in the banded iron formations deposit in Kryvyi Rih, Ukraine

Anatolyi Berezovsky [a], Jadwiga Pieczonka [b,*], Adam Piestrzynski [b]

[a] Kryvyi Rih National University, 11Vitaliy Matusevych St, Kryvyi Rich 50027 Ukraine
[b] AGH-University of Science and Technology, Faculty of Geology, Geophysics and Environmental Protection, Al. Mickiewicza 30, 30-059 Krakow, Poland

A R T I C L E I N F O

Keywords:
Au-Ag-Sb-Cu-Pb mineralization
First discovery
BIF
Kryvyi Rih

A B S T R A C T

Since the beginning of iron mining in Kryvyi Rih in 1881, gold was a target of interest. Exploration for gold began in 1936. As a result, many gold occurrences were discovered. In this paper, regional geology of the gold mineralization and the iron deposit details are also described for better understanding of the position of hydrothermal mineral association. Gold - silver and polymetallic mineralization was found in the iron ore horizon in the Ingulets operating iron open pit. A new association of gold and Sb-bearing sulfosalts is described. Gold occurs in an association with arsenopyrite, pyrite, and pyrrhotite in quartz-arsenopyrite veins type mineralization discovered in the Ingulets quarry. Gold was found as minute inclusions in arsenopyrite and as inclusions in Ag-Sb-, Pb-Sb-, Ag-Pb-Sb- sulfosalts. Based on both ore microscope and EMP measurements, the following minerals have been identified: arsenopyrite, pyrite, pyrrhotite, tetrahedrite, freibergite, sphalerite, chalcopyrite, galena, stibnite, plagonite, zinkenite, fuloppite, miargyrite, chalcostibite, andorite, and native Sb and electrum. It is the first discovery of Ag-Sb-Cu-Pb mineral association in the whole Kryvyi Rich structure. In this paper quantitative EMP measurements of all new minerals of the newly discovered association are presented. The baro-acoustic decrepitation analyses of the massive arsenopyrite and pyrite showed temperature formation ranging between 450 °C and 650 °C with an average of T ~ 585 °C. Based on mineralogical investigations, ore occurrences are considered as the product of high and middle temperature hydrothermal processes.

1. Introduction

The Kryvyi Rih iron ore basin (KRIOB) is one of World-class BIF deposits. Total volume of reserves and resources is calculated to be 70 Gt. Annual production reaches 7 Mt of fresh steel and 17 Mt of ore containing 35 wt% iron. It is located in the centre of the Ukrainian Shield and is confined within the Kryvyi Rih-Krementchuk fault zone. The Ukrainian Shield is composed of 6 Megablocks and 3 three suture zones (Gurskyi, 2002). One of these suture zones separates two megablocks of the crystalline shield - the Early Proterozoic Ingul (or Kirovograd) and Mesoarchean Middle Dnieper (or Subdnieper).

Recently, the eastern part of the Ingul Megablock has been recognized as a separate geostructural unit - the Ingulets-Kryvyi Rih suture zone. Thus, according to the latest interpretation, the KRIOB is a narrow, northerly-trending, strip of Archean – Phanerozoic aged metamorphic rocks about 100 km long and 0.5 to 18 km wide located between the Mesoarchean Middle Dnieper Megablock to the east and the Ingulets-Kryvyi Rog zone to the west.

The Mesoarchean Konska Series, as well as the Paleoproterozoic Kryvyi Rih series and the Gleevatska suite, are metamorphosed volcanic and volcanogenic-sedimentary rocks. The Phanerozoic is represented by Cenozoic sedimentary rocks.

The Konska Series is not subdivided. The Kryvyi Rih series is divided into four suites (formations) - the Novokryvorizka, Skelevatska, Saksaganska, and Gdantsevska.

The Novokryvorizka Suite overlies the Konska Series with angular unconformity. It is mainly composed of amphibolites (metabasites), various chlorite and micaceous schists.

The Skelevatska Suite, conformably overlying the Novokryvorizka Suite, is composed of three sub-suites: lower, middle and upper. The lower sub-suite is composed mainly of metaconglomerates and metasandstones. The lower part of the middle sub-suite is also composed of metaconglomerates and metasandstones, while the upper part consists of phyllites (quartz-mica schists). The upper sub-suite is composed mainly of talc schists.

The Saksaganska Suite, conformably overlying the Skelevatska Suite,

* Corresponding author.
E-mail addresses: berez-08@mail.ru (A. Berezovsky), jpieczon@agh.edu.pl (J. Pieczonka), piestrz@agh.edu.pl (A. Piestrzynski).

https://doi.org/10.1016/j.precamres.2021.106326
Received 19 February 2021; Received in revised form 12 July 2021; Accepted 13 July 2021
Available online 2 August 2021
0301-9268/

is the productive iron ore strata of the KRIOB. The complete sequence includes seven interbedded ferruginous and schistose horizons. The Suite is divided into three sub-suites: lower (the first, and the second schist horizons and first and second ferruginous horizons), middle (third, fourth schist horizons and third ferruginous horizon) and upper (fifth, sixth, seventh schist horizons and fourth, fifth, sixth, seventh ferruginous horizons). The ferruginous horizons are composed of magnetite, magnetite-silicate, silicate-magnetite quartzites. The schist horizons are composed of various mineral varieties of the metamorphic beds.

The Gdantsevska Suite completes the Kryvyi Rih Series and overlies the Saksaganska Suite with angular unconformity. It is comprised of a variety of chlorite schists, micaceous schists, metasandstones, metaconglomerates, ferruginous quartzites, rich iron ores, quartz-carbonate rocks and dolomite marbles. Metaconglomerates, metasandstones, and various biotite schists of the Gleevatska Suite overlie the Kryvyi Rih Group.

The sedimentary cover of the KRIOB is composed of Cainozoic rocks of the Paleogene, Neogene and Quaternary systems, the thickness of which reaches 150 m.

In 2014, during the exploitation of the iron ore deposit in the opencast mine of the Ingulets Ore Mining and Processing Plant in Kryvyi Rih, Ukraine, on the north-eastern edge of the open cast, at a depth of minus 134 m b.s.l, in Proterozoic quartz-mica schists (phyllites) of the Skelevatska (Skelevatskaja) Suite, a section with metasomatic alteration was discovered. Phyllite in this section contains plenty of scattered arsenopyrite crystals and massive aggregates. Arsenopyrite crystals occur in a scattered through in the main mass of phyllites, as well as in conjunction with hydrothermal quartz veins. A fragment of phyllite with metasomatic changes up to 20 m thick is located at the intersection of mining works of the 55th vertical and 73rd mining geodesy polygons. Gold, and silver, mineralization associated with a polymetallic suit, mostly copper and other minerals, were found while examining massive arsenopyrite and surrounding rocks.

Phyllites occur in the middle sub-suite of the Skelevatska Suite of the Kryvyi Rih Series in the stratigraphic section of ferruginous quartzite formations in the Kryvyi Rih Basin. Below outcropping metasandstones, there is the lower sub-suite is followed by talc schist, of the upper sub-suite of the Skelevatska Suite. The cover consists of talc schists of the upper sub-suite of the Skelevatska Suite. Skelevatska rocks rest on amphibolites (metabasites) of the Novokryvorizka (=Novokrivorozhskaja) Suite or directly on the basement composed of the Saksagan plagiogranites of the Konska (=Konskaja) Series of the Dnieper Block of the Ukrainian Shield. Over the rocks of the Skelevatska Suite, there is a series of Lower Proterozoic formations, which consists of alternating ferruginous and schist horizons of the Saksaganska Suite (in the Ingulets deposit, five schists horizons and five ferruginous horizons have been identified) that begins with the first schists horizon.

Since 1936 gold prospecting in the area of Kryvyi Rih and its surroundings has been carried out on a systematic basis. Up to now, despite identification of many occurrences of gold and manifestations of sulphide mineralization. Gold occurrences are recognized in different lithostratigraphic units in all rocks of the KRIOB. Six generations of gold mineralisation have been recognized during these investigations (Sukach et al., 2013) as follows:

The first generation consists of detrital gold, which occurs in metaconglomerates, metasandstones, quartzites and different schist types of the lower and middle Skelevatska Suite. Gold was precipitated from solutions released during regional metamorphism.

The gold of the second generation was classified as orogenic (Sukach et al., 2013). After this metamorphic period, gold was transported away from the quartz veins and precipitated in fissure zones of the Kryvyi Rih Series.

The third gold type is related to a Na-metasomatic processes. This gold is located within the quartz-rich metasomatic bodies, which form an aureole surrounding riebeckite-albite-aegirine metasomatites of the Saksaganska Suite.

Gold which was documented within the hydrothermal-metasomatic rocks located between amphibolites of the Novokryvorizka Suite and granitoids was classified as the fourth generation. As a result of similar processes veins containing quartz, calcite, pyrite, pyrrhotite, albite and chlorite were formed.

Gold of the fifth generation was identified in supergene oxidation zones developed on the Kryvyi Rih Series and the accompanying granitoids. During the weathering processes gold was liberated from altered sulphides, carbonates and silicates.

Gold of the sixth generation occurs in alluvial sediments deposited along Ingulets, Saksagan and Yellow River and their tributaries.

The content of gold in the iron ores of the Saksaganska Suite is similar to its Clarke concentration (3–4 ppb) and only in a few places it is 3–3.5 times greater than that in this horizon. The highest number of cases of identification of anomalously high gold content in the Kryvyi Rih basin was recorded in rocks from the first and second schist horizons and the first ferruginous horizon of the Ingulets deposit. Apart from that, in the Ingulets deposit, at the contact of rocks of the Gdantsevska (=Gdantsevskaja) Suite and Saksaganska Suite, the content of secondary (epigenetic) gold is over ten times higher than the Clarke concentration (Metchnikov, 2000). In practice, sediments of the third schist, third ferruginous and fourth schist horizons do not contain any gold. In the rocks of the fourth ferruginous horizon, gold is associated with areas of epigenetic pyritization. In the fifth ferruginous horizon, gold was found in the oxidation zones of the ferruginous ore weathering crust (Lazarenko et al., 1977).

It has been found that the highest content of gold in the Ingulets deposit occurs in amphibolites of the Novokryvorizka Suite, in metaconglomerates of the Skelevatska Suite, in high-grade iron ores and in sulphide zones connected with the contact between the fifth ferruginous horizon and schists as well as with ore-free quartzites of the Gdantsevska Suite.

In amphibolites of the Novokryvorizka Suite in the Ingulets deposit, gold is associated with pyrite, chalcopyrite, and less frequently with pyrrhotite of upper zones of the old weathering cover. Gold in the amphibolites was probably formed in conditions of hypo-genesis.

It has been found that in rocks of the Skelevatska Suite, the maximum content of gold is associated with metaconglomerates. The gold content and the size of nuggets increases toward the base of the metaconglomerates. Gold in metaconglomerates is in a free state and has the shape of fine-scale dendrites. This is associated with sulphides (Lazarenko et al., 1977). In addition, it has been found that in these metaconglomerates, gold occurs as inclusions (less than 0.001 mm) within pyrite, ilmenite, garnet, vein quartz and quartz-sericite cement. It is assumed that two genetic types of gold mineralisation are identified: hydrothermal-metasomatic (pyrite, arsenopyrite, vein quartz, this work) and metamorphogenic (ilmenite, garnet) (Sukach et al., 2013). In the metaconglomerate-metasandstone series, the gold mineralization is associated with the cementing material, but not with clastic components. The average gold content is 0.1–0.2 g per ton. No increased gold content has been observed in phyllites and in talc schists.

In high-grade iron ores in the Ingulets deposit, the increased gold content was identified during their testing in the Central and No. 10 mines laboratories. In these ores, gold is associated with the faults that separate the rocks of the Saksaganska and Gdantsevska Suites, and is connected with the overlaying hypogenic sulphidation in the form of isolated inclusions and partings. Originally, gold was associated with pyrite – it occurred mainly in a finely dispersed form. The oxidation of pyrite was accompanied by separation of native gold and its accumulation in hematite. Low assays of gold, morphology of its inclusions and a close relationship with sulphides allowed linking of the gold mineralization in high-grade ores of the Ingulets deposit with the infiltrating circulation of sulphide waters enriched with gold (Lazarenko et al., 1977).

In this paper, results of the investigation of arsenopyrites occurrences in phyllites characterized by metasomatic changes belonging to the Skelevatska Suite, as well as their relationship with gold and silver are discussed. The occurrence of gold and silver associated with arsenopyrite, other sulphides and sulfosalts in phyllites of the Skelevatska Suite in the Kryvyi Rih basin has been identified for the first time.

2. General Geology of the Kryvyi Rih mining area

The Ukrainian Shield is the most important craton in the world with respect to large iron deposit (BIF-type) (Belevcev et al., 1981).

Kryvyi Rih Iron Ore Basin (KRIOB) is located in the middle part of southern slope of the Ukrainian Shield (Fig. 1). It represents an outcropping suite of ferruginous quartzite 7 km wide along the strike from north to south through Kryvyi Rih city and the Ingulets and Saksagan Rivers. The length of this structure containing BIF is 85 km. This zone is related to a boundary between two mega blocks: Western Ingulets Block (very often called Kirovograd Block) which comprises Lower Proterozoic volcanic-sedimentary and granitoid rocks, and Eastern Block called Middle Dnieper Block composed of early Archaean plagiogranites located within the greenstone belts of late Archaean age.

The BIF ores were discovered on the bank of Ingulets River by Vasiliy Zuev and described by him first in 1781. Archaeological artefacts suggest an earlier epoch of mining works and smelting. The beginning of modern mining was in 1881 year (Belevcev et al., 1981).

Three major lithostratigraphic complexes are recognized within the ore field: Archean granites and migmatites, Proterozoic crystalline schist and Cenozoic sediments. Crystalline schists are in some places cut by Proterozoic granites and diabase dykes of late-Proterozoic age (Gurskiy, 2002; Kulish and Gurskiy, 2005).

The Konska Series, forms the lowest part of the KRIOB geological section. The Series, which is not segmented in this area, is composed mostly of quartz-hornblende schists and amphibolites. The thickness of this unit reaches 700 m in the southern part and 1100 m in the northern sector (Konska Series is identified within the KRIOB only by some researchers). Other authors classified rocks of the Konska Series as part of the Novokryvorizka Suite.

An angular unconformity separates the Konska Series from the overlying Kryvyi Rih Series. In stratigraphically ascending order, this Series is composed of the Novokryvorizka, Skelevatska, Saksaganska, Gdantsevska and Gleevatska suites (Table 1).

The Novokryvorizka Suite is composed of quartz-biotite-chlorite and quartz-hornblede-biotite schists. Metasandstones and meta-gravels are locally present. Thickness of this unit is in the range 20–300 m.

The Skelevatska Suite lies conformably on the Novokryvorizka Suite and is divided into three Sub-suites: Lower, Middle and Upper. The Lower Sub-suite comprises quartz metasandstones, meta-gravels, and metaconglomerates. Total thickness amounts to 1–160 m. The Middle Sub-suite is composed of biotite-quartz, quartz-biotite, sericite-biotite and sericite-quartz-biotite phyllites. Thickness of these beds is 50–80 m. The Upper Sub-suite is comprised of talc schists and actinolite, tremolite and talc-carbonate rocks and its thickness amounts to 5–360 m.

The Saksaganska Suite is composed of ferruginous quartzite intercalated with various crystalline schists. The most complete geological section through this unit comprise seven ferruginous and schist horizons. Thickness of individual horizons can reach 450 m. Saksaganska Suite starts with the first schist horizon and ends with seven ferruginous horizons. Ferruginous horizons are composed of hematite-magnetite, magnetite, silica-magnetite and carbonate–silicate quartzites. Schist horizons consist of metamorphosed silt and sandy clays converted into cummingtonite-biotite, carbonate-chlorite, sericite-chlorite, muscovite-biotite crystalline schists. Both the fifth and sixth ferruginous horizons comprise hematite and magnetite quartzite. Total thickness of the Saksaganska Suite is very variable and ranges from 40 to 1300 m (Gurskiy, 2002).

In the Gdantsevska Suite, three Sub-suites are documented: Lower, Middle and Upper.

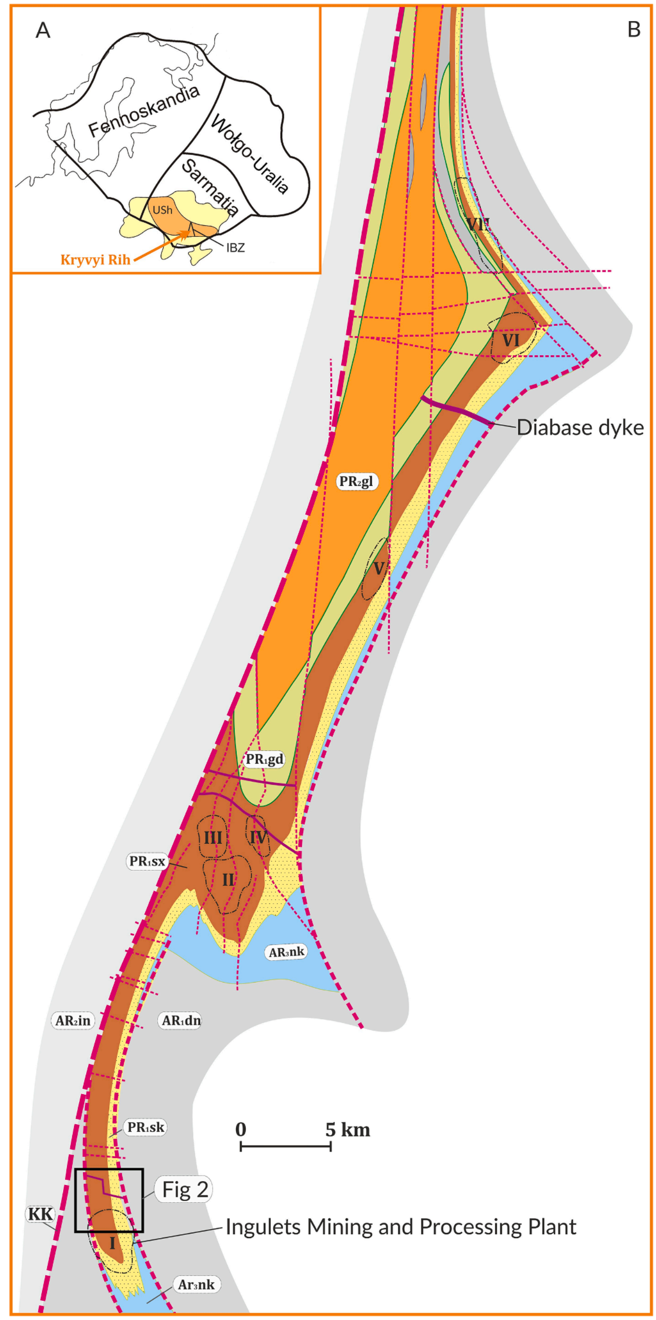

Fig. 1. Geological schematic map of Precambrian beds of the Kryvyi Rih Iron Basin. A-Position of Ukrainian Shild (USh) in Eastern European Platform. IBZ – inter-block zone. B-Geological schematic map of Precambrian beds of the Kryvyi Rih Iron Basin. **Ar_1dn** – rock of the Middle Dnieper Block; **Ar_2in** – rock of the Ingulets Block; **Ar_3nk** – rocks of the Novokryvorizka Suite; **PR_1sk** – rocks of the Skelevatska Suite; **PR_1sx** – rocks of the Saksaganska Suite; **PR_1gd** – rocks of the Gdantsevska Suite; **PR_2gl** – rock of the the Gleevatska Suite; I-VII- active open pits: II – Southern Mining and Processing Plant, III and IV – Novokryvorizky Mining and Processing Plant, V – Central Mining and Processing Plant, VI and VII – Northern Mining and Processing Plant; **КК** – Kryvyi Rih – Krementchuk deep tectonic zone.

The Lower Sub-suite is mostly composed of magnetite-quartz-chlorite schists, quartz-sericite-chlorite schists, metasandstones, ferruginous quartzite, rich magnetite and martite ores. Average thickness is 300 m.

The Middle Sub-suite is mostly composed of graphite-mica schists,

Table 1
Lithological section of the crystalline complex including deposit beds of the KR formation (after Gurskiy, 2002).

Maximal thickness	Suite/horizons	Lithology of the KR formation
2500 m	Gleevatska Suite **(PR_2gl)**upper **(PR_2gl_3)**	• quartz-biotite schists • graphite-mica schists, biotite- quartz-carbonate schists, dolomite, marbles
	middle **(PR_2gl_2)**	• magnetite-quartz-chlorite schists, quartz-sericite-chlorite schists, meta-sandstones, ferruginous quartzite, rich magnetite and martite ores
	lower **(PR_2gl_1)**	
		unconformity
1,750 – 2,000 *m*	Gdantsevska Suite **(PR_1gd)**upper **(PR_1gd_2)**	• quartz-biotite schists, metasandstones, metaconglomerate lens • metaconglomerates, quartz-biotite schists
	lower **(PR_1gd_1)**	
500–700 m	Saksaganska Suite (PR1sx) VIIth ore horizon (PR1sx7f)	**magnetite-carbonate–silicate quartzites and silicate- carbonate-magnetite quartzites with quartz-chlorite schists, amphibole-quartz-chlorite schists, chlorite- carbonate-quartz-biotite schists, martite quartzites, martite quartzites with iron mica (hematite), goethite- hematite quartzites, goethite-hematite quartzites, goethite-hematite-martite quartzites**
50–60 m	VIIth schists horizon **(PR_1sx^{7s})**	magnetite-carbonate-amphibole schists, and magnetite- chlorite-amphibolite schists, ribeckite-magentite schists with barren quartzites
30–300 m	**VIth ore horizon (PR_1sx^{6f})**	**magnetite quartzites, silicate-magnetite quartzites, and carbonate-magnetite quartzites**
50–180 m	VIth schists horizon **(PR_1sx^{6s})**	cummingtonite-chlorite and biotite-chlorite schists Magnetite occurring as a dispersed crystals in host rocks
30–250 m	**Vth ore horizon (PR_1sx^{5f})**	**magnetite-carbonate–silicate quartzites, carbonate- silicate-magnetite quartzites, magnetite quartzites and ferruginous-mica-magnetite quartzites**
50–120 m	Vth schists horizon **(PR_1sx^{5s})**	chlorite-sericite-quartz schists, and amphibolite- chlorite-biotite schists with graphite
700 m	**IVth ore horizon (PR_1sx^{4f})**	**silicate-carbonate-magnetite quartzites, carbonate- magnetite quartzites, silicate-magnetite quartzites**
300 m	IVth schists horizon **(PR_1sx^{4s})**	sericite-chlorite schists, sericite-biotite-chlorite schists, biotite-chlorite schists with graphite, intercalated with barren quartzites
50 m	**IIIth ore horizon (PR_1sx^{3f})**	silicate-magnetite quartzites
140 m	IIIth schists horizon **(PR_1sx^{3s})**	graphite-chlorite-biotite schists intercalated with barren quartzites
150 m	**IIth ore horizon (PR_1sx^{2f})**	magnetite quartzites and silicate-carbonate-magnetite quartzites
60 m	IIth schists horizon **(PR_1sx^{2s})**	biotite-chlorite-amphibolite schists intercalated with barren quartzites
400 m	**Ith ore horizon (PR_1sx^{1f})**	magnetite quartzites, silicate-magnetite quartzites, carbonate–silicate-magnetite quartzites
300 m	Ith schists horizon **(PR_1sx^{1s})** Ag-Sb-Au	amphibolite-chlorite-biotite schists intercalated with barren quartzites
60–350 m	Skelevatska Suite **(PR_1sk)**	
	upper (10–20 m) **(PR_1sk_3)**	talc schists and actinolite, tremolite and talc-carbonate rocks
	middle (40–60 m) **(PR_1sk_2)**	biotite-quartz, quartz-biotite, sericite-biotite and sericite-quartz-biotite phyllites. **Arsenopyrite – Sb-Ag sulphosalts and gold**
	lower (40–50 m) **(PR_1sk_1)**	quartz metasandstones, meta-gravels, and metaconglomerates. ***unconformity***
700–1100 m	Novokryvorizka Suite-Konska Series **(AR_3nk)**	mostly quartz-hornblende schists and amphibolites

biotite- quartz-carbonate schists, dolomite, and marbles. Average thickness of this sub-suite is 450 m.

The Upper Sub-suite is mostly composed of quartz-biotite schists. Average thickness reaches 400 m.

The Gleevatska Suite is composed of quartz-feldspar metasandstones, metaconglomerates and biotite schists, with total thickness of 2500 m.

Proterozoic ferruginous-silicate formations are covered by the Palaeogene, Neogene and Quaternary sandy clay and carbonate beds.

3. Geological setting of the Ingulets deposit

The geological structure of the Ingulets deposit includes rocks of four Proterozoic geological suites: the Novokryvorizka, Skelevatska, Saksaganska and Gdantsevska suite (Figs. 1, 2, 3).

The Novokryvorizka Suite consists of amphibolites. In the southern and eastern parts of the deposit, amphibolites form a continuous belt within the Skelevatska Suite, while in the western part they are developed only at separate locations. Sediments of this suite occur inconsistently on Archaean rocks of the Konska Series, while their thickness is 4–50 m (Fig. 3).

Skelevatska Suite. The Lower and Middle Sub-suites of the Skelevatska Suite are represented by intercalations of quartz-sericite metasandstones, metagravelstones, metaconglomerates, quartz-mica schists (phyllites) and mica quartzites. Interbeds of quartzites and metasandstones with mica schists are observed in this Suite. The thickness of this suite varies from 60 m to 350 m.

The Upper Sub-suite of the Skelevatska Suite is composed of talc schists and actinolite, tremolite and talc-carbonate rocks. Their thickness varies from 40 m to 160 m. The occurrence of alkaline metasomatism (albitization) is observed in these schists.

Saksaganska Suite. This Suite begins with the first schist horizon (with a thickness of 20–60 m) of quartz-biotite schist. These underlie the first ferruginous horizon with a thickness of 10–20 m. This horizon consists of magnetite-cummingtonite and cummingtonite-magnetite quartzites. They are overlain by rocks of the second schist horizon, represented by grey-green garnet-cummingtonite and garnet-biotite schists with interbeds of barren quartzite. The thickness of this horizon is 10–40 m. Above it, there occurs low-grade silicate-magnetite, magnetite-silicate and red magnetite band-like quartzites with a thickness of 30–115 m, which form the second ferruginous horizon. Above, there are rocks of the third schist horizon represented by garnet-biotite-cummingtonite schists with intercalation of barren quartzites. At this horizon, abundant sulphide mineralization (pyrite, pyrrhotite) occurs. The third ferruginous horizon, which occurs above, is represented by magnetite-silicate and silicate-magnetite quartzites. Its thickness varies from 0 to 30 m (in some sections, this horizon wedges out). The fourth schist horizon, where garnet-biotite, quartz-biotite and garnet-cummingtonite schists occur, overlies the third ferruginous horizon. The thickness of this horizon is 0–10 m. The fourth ferruginous horizon has a thickness of 20–100 m. It consist of magnetite quartzites. In the rocks of this horizon, the processes of alkaline metasomatism (aegirinization, riebeckitization

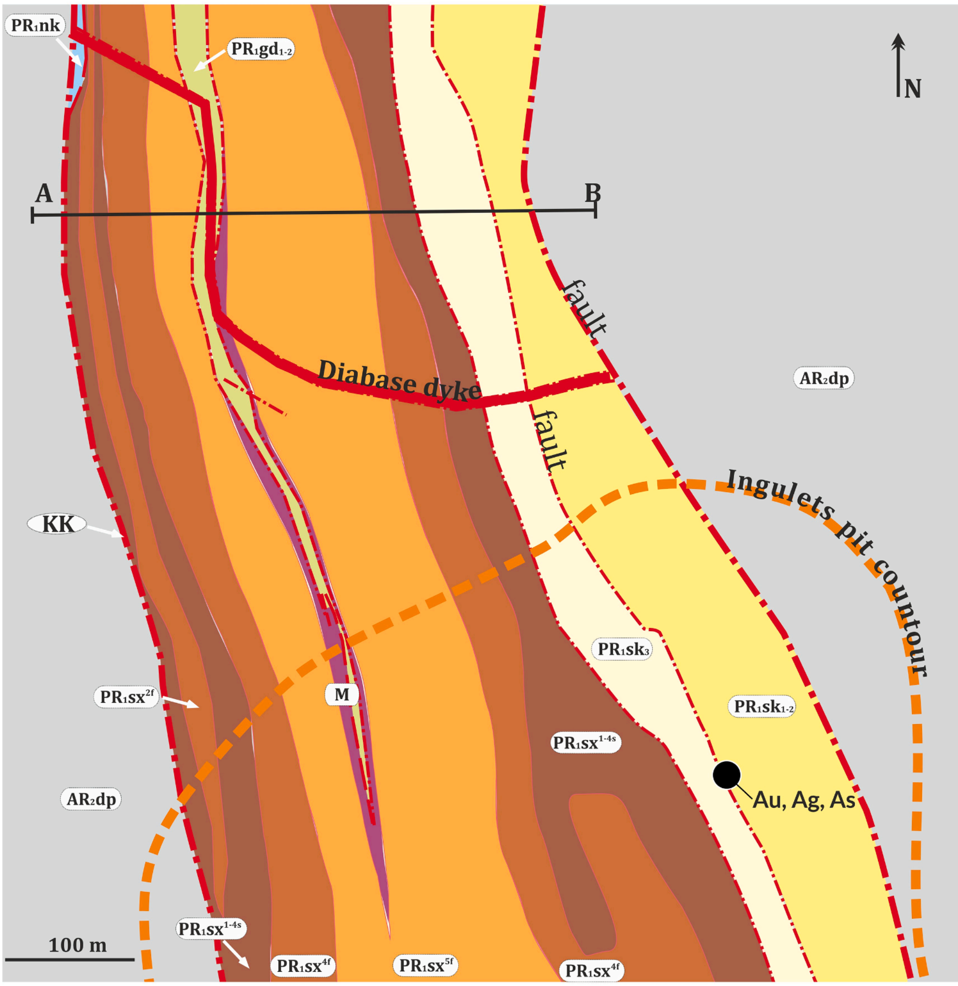

Fig. 2. Geological map of Precambrian beds of the Northern part Ingulets Mining and Processing Plant, section A from Fig. 1. **PR$_1$nk** – Novokryvorizka Suit; **PR$_1$sk**$_{1\text{-}2}$ – Skelevatska Suite, lower and middle subsuite; 3 **PR$_1$sk**$_3$ – talc-carbonate rocks of the upper subsuite, the Skelevatska Suite; **PR$_1$sx$^{1\text{-}4s}$** – fourth Schists horizons, the Saksaganska Suite; **PR$_1$sx^{4f}** – rocks of the fourth Ferruginous horizons, the Saksaganska Suite; **PR$_1$sx^{5f}** – rocks of the fifth Ferruginous horizons, the Saksaganska Suite; **M** – rich Ferruginous ore of the crust of weathering of the Saksaganska Suite; **PR$_1$gd** – rocks of the Gdantsevska Suite; **Ar$_2$dp**–rocks of the Middle Dnieper Block; **A-B** – the line of geological section; **Au, Ag, As** – location of the arsenopyrite body.

and carbonization) are developed. Above, there is the fifth schist horizon with a thickness of 10–15 m. It is represented by silicate-magnetite and magnetite-silicate quartzites. Interbeds of magnetite and hematite-magnetite quartzites (Gurskiy, 2002) represent the fifth ferruginous horizon.

Recently, some researchers (Gurskiy, 2002; Sukach et al., 2013) started to distinguish the seven schist and seven ferruginous horizons (Table 1) in the Saksaganska Suite of the Ingulets deposit. The occurrence, in the central part of the fifth ferruginous horizon, of 3–4 schist beds with garnet-cummingtonite-biotite-quartz-chlorite composition (1 to 5 m thick), intercalated with 2–3 beds of ferrous-mica magnetite and magnetite quartzites (1 to 12 m thick), provided a basis for separating the independent sixth schist horizon. The sixth ferruginous horizon is separated from the fifth ferruginous horizon and consists mainly by ferrous-mica-magnetite and magnetite-ferrous-mica quartzite. In the zones of contact with the sixth schist horizon, thin seams and lenses of silicate-magnetite and sometimes magnetite-silicate quartzite have been identified. Both the upper part of formations of the sixth ferruginous horizon and the adjoining formations of the sixth schist and fifth ferruginous seams constitute a zone of intense hypergenic changes, which consists of ferrous-mica-martite, martite-ferrous-mica, martite and hematite-martite quartzites. The thickness of the horizon varies from 10 m to 200 m.

Gdantsevska Suite. Sediments of this suite occur with angular unconformity on the fifth horizon of the ferruginous Saksaganska Suite and are represented by graphite-sericite-chlorite and biotite-quartz schists as well as by mica quartzites. In the lower part, among barren schists and quartzites, lenticular bodies of high-grade iron ores occur. The thickness of the seam is 5–70 m.

Rocks of the above mentioned suites of Palaeoproterozoic are cut in places with Neoproterozoic diabase dikes. These dikes are associated with complex tectonic discontinuities. The main minerals of the diabase rocks are plagioclase and pyroxene, while secondary minerals include ilmenite, chlorite, sericite, and leucoxene. The thickness of the diabase dikes reaches 30 m.

4. Tectonic features

The Ingulets deposit of ferruginous quartzites is structurally related to the erosional exposure of the core of the Likhmanovska syncline (Belevcev et al., 1962).

The eastern limb of the syncline within the boundaries of the deposit is characterized by a western sub-meridional strike and often has a reverse dip. The western limb is cut by the Western overthrust (nappe). For this reason, the fold has an asymmetrical structure. The cross-section of the closure of the Likhmanovska syncline has the shape of a trough. A characteristic feature of the syncline is a steep dip of the hinge in the northern direction (up to 30–35°). In limbs of the Likhmanovska syncline, there are developed asymmetrical drag folds. Its eastern limb has a complex structure due to zones of brecciation and separate small folds. A steep dipping of beds is observed (Belevcev et al., 1962).

The axis of the main syncline is represented by a series of axes of small folds. They have an echelon arrangement, because of which the axis of the main syncline in the direction from the south to the north gradually shifts westward.

In addition to folds of various size, faults are also widespread within

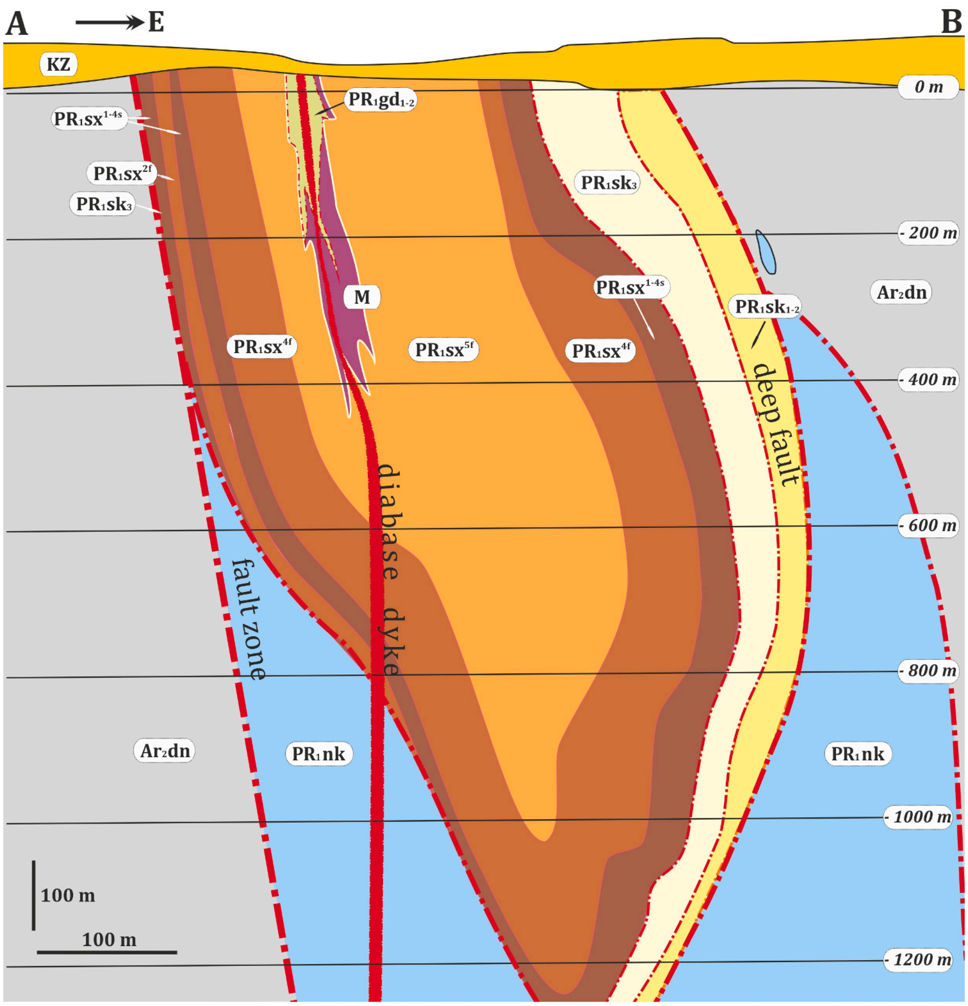

Fig. 3. Geological section along of the line A-B from Fig. 2. **Ar_2dn** rocks of the of the Middle Dniper Block; **PR_1nk** – rocks of the Novokryvorizka Suite; **$PR_1sk_{1\text{-}2}$** – meta-gravels, meta-conglomerates and phyllite of the Skelevatska Suite; **PR_1sk_3** – talc-carbonate rocks, the Skelevatska Suite; **$PR_1sx^{1\text{-}4s}$** – rocks of the first – fourth Schists horizons, the Saksaganska Suite; **PR_1sx^{4f}** – rocks of the fourth Ferruginous horizons, the Saksaganska Suite; **PR_1sx^{5f}** – rocks of the fifth Ferruginous horizons, the Saksaganska Suite; 8 **M** – massive ferruginous ore of the crust of weathering of the Saksaganska Suite; **PR_1gd** – rocks of the Gdantsevska Suite; KZ – Cainozoic cover.

the boundaries of the Ingulets deposit. The Western fault has the greatest significance in the structure of the deposit. Within the boundaries of the deposit, its thickness of 12–15 m is represented by cataclastic, intensively weathered ferruginous rocks with a large number of veins of quartz, carbonate, carbonate-quartz, and microcline-quartz. The strike of the main fault plane has a sub-meridional direction, while the western dip is at an angle of 75–85°.

The central and eastern parts of the deposit are disturbed by a series of faults, which are characterized by a sub-meridional strike and a steep dip in the western direction, less frequently in the eastern direction. The largest fault in the central part of the deposit is represented by a zone of fractures with slickensides. The thickness of its zone is 0.5–0.7 m, while in the northern part of the open pit – up to 15 m. Some fissures are filled with quartz with a small amount of sulphides (pyrite, pyrrhotite), carbonates (calcite, dolomite, and ferro-dolomite), silicates (chlorite, ferrous talc, seladonite, stilpnomelane, cummingtonite and biotite). The thickness of the veins varies from 1–2 to 40–50 cm.

One of the specific structural features of the ferruginous series of the Likhmanovska syncline is the intensive development of slide fissures, tears, and cleavage. Usually, the fissures are of open type, but often they are also filled with quartz, carbonates, silicates, ore minerals (mostly iron mica, and more rarely magnetite). A characteristic feature of the intense fissure zones is an increased content of admixtures of elements (Mn, Cu, Ni, Mo, Ti, Cr, Zn) in the ferruginous rocks.

The layers of the sedimentary cover rocks are located on formations of the crystalline basement with a low dip (3–5°), generally dipping in the southern direction.

5. Gold occurrences in the Kryvyi Rih structure

Twenty-nine gold occurrences are documented within the Kryvyi Rih structure (Fig. 4) and adjacent areas. Since 1936 the occurrences of gold have been investigation targets. The highest concentrations of visible gold mineralization has been described from the pyrite zones at the contact of Saksaganska and Gdantsevska Suites, and from a pyrite mineralization zone located in lowermost section of magnetite rich of Gdantsevska Suite as well as in the upper sections of pyrite-rich graphite schists (Fig. 4; Table 2, no 13, 15, 16, 17, 19 and 21) (Evtekhov et al., 1999). The presence of gold (1–14.5 ppm) was also noted in the waste from mineral dressing technological lines (Fig. 4; Table 2, no 1, 8, 10, 18 and 25) (Kozin, 2014).

The economic concentration of gold have been documented in the Yellow Water uranium deposit (Fig. 4). Gold is concentrated in lenses-type bodies 2–27 m thick characterized by low temperature metasomatites composed of clays and secondary, low temperature quartzites (Yushin and Butyrin, 2009). These zones contain also intensive brecciated magnetite quartzite. A zone containing pyrite-gold mineralization is 8 km long and 100–200 m wide is located in the Kr-K deep tectonic zone. Within the metasomatites thin (up to 0.5 m thick) mineralized zone have been found. Some sections of these zones contain up to 10–49 ppm of Au. Gold bearing zones contain also pyrite (5–7%) and minor arsenopyrite, chalcopyrite, sphalerite and galena. Zinc - silver anomalies are observed within the gold containing sections. Gold was recognized as electrum containing 70% of Ag in average. In this deposit Ag-Au-As-Cu-Zn-Bi-Te paragenesis has been described (Yushin and Butyrin, 2009).

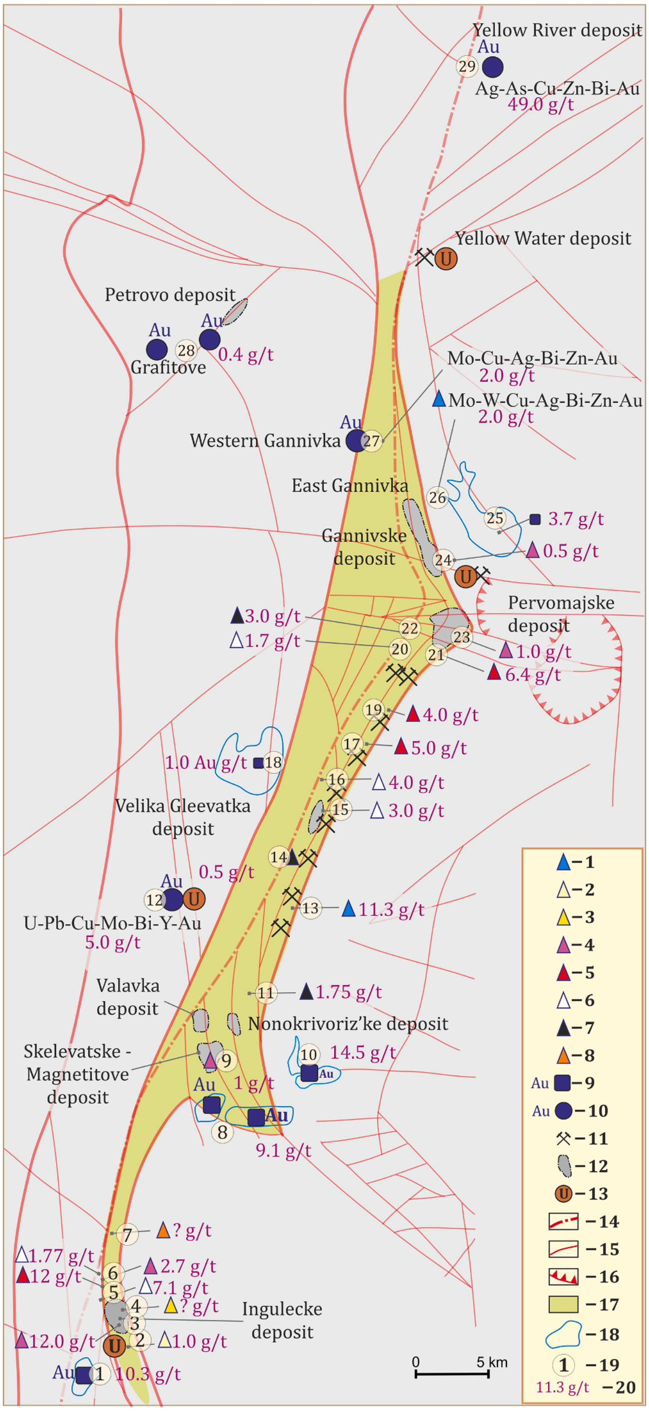

Fig. 4. Gold mineralization within the Kryvyi Rih Iron Basin. 1 – gold mineralization in the rocks of the Novokryvorizka Suite; 2 – gold mineralization in the meta-conglomerates of the Skelevatska Suite; 3 – gold mineralization in the phyllite of the Skelevatska Suite; 4 – gold mineralization of the rocks of the Schists and Ferruginous horizons of the Saksaganska Suite; 5 – gold mineralization in contact zone Saksaganska Suite and Gdantsevska Suite; 6 – gold mineralization of the low part of the Gdantsevska Suite; 7 – gold mineralization of Upper Part of the Gdantsevska Suite; 8 – gold mineralization in Quaternary alluvium; 9 – techno-genetic gold deposits; 10 – other types of the gold mineralization; 11 – deep mine; 12 – quarry; 13 – uranium deposits; 14 – Kryvyi Rih – Krementchuk deep tectonic zone; 15 – dislocation with a break of continuity; 16 – circular structure; 17 – territory of Kryvyi Rih Iron Ore Basin; 18 – sludge storehouse; 19 – gold mineralization (name of the gold mineralization see in text of the article); 20 – maximum gold concentration.

Table 2
Gold occurrences within the Kryvyi Rih structure.

no	Geological unit, deposit	Rock type	Au [ppm]	References
1	Saksaganska Suite (**PR$_1$sx**), Ingulets deposit	waste from mineral dressing plant	up to 10.3	Kozin, 2014
2	Skelevatska Suite **(PR$_1$sk)**, Nikolo-Kozel'sk deposit	metaconglomerates with U, Ag, Pb, Ni, Cu, Mo, Bi mineralization	up to 1.0	Grechishnikov and Sakhatsky, 1973
3	Saksaganska Suite (**PR$_1$sx**), Ingulets deposit	Q, py-asp, veins at carbonate-magnetite quartzites	up to 12	Machado and Yurtaeva, 1997
4	Skelevatska Suite, middle zone **(PR$_1$sk$_2$)**, Ingulets deposit	phyllite with massive asp and py, cpy, sulphosalts mineralization	As, Au, Ag, Zn, Cu, Pb, Bi,	this work
5	Lover Part of the Gdantsevska Suite (**PR$_1$gd$_1$**), Ingulets deposit, Mine Central	Crust of weathering of rich ferriferous ore	up to 7.1	Velikanov et al., 2010
6	Saksaganska Suite (**PR$_1$sx**), Ingulets deposit, Mine no 10	fissures of I schist horizons, I Ferruginous horizons and II schist horizons,	up to 2.7	Pletnev, 1972
6	Contact of Saksaganska Suite (**PR$_1$sx**) and Gdantsevska Suite (**PR$_1$gd**), Ingulets deposit, Mine no 10	sulphides mineralization	up to 12.0	Velikanov et al., 2010
6	Lover Part of the Gdantsevska Suite (**PR$_1$gd$_1$**), Ingulets deposit, Mine no 10	Crust of weathering of rich ferriferous ore	up to 1.77	Velikanov et al., 2010
7	Kryvyi Rih Iron Ore Basin, Quaternary deposits Zelenoe village	Quaternary alluvia sands	?	Kozin, 2014
8	Saksaganska Suite (**PR$_1$sx**), Skelelevatske Magnetitove deposit	waste from mineral dressing plant	up to 9.1	Kozin, 2014
9	Saksaganska Suite (**PR$_1$sx^{4s}**), Skelevatske Magnetitove deposit	fissures of IV Ferruginous horizon	up to 1.0	Latys and Shaposhnikov, 1974
10	Saksaganska Suite (**PR$_1$sx**), Nonokrivoriz'ke deposit	waste from mineral dressing plant	up to 14.5	Kozin, 2014.
11	Gdantsevska Suite (**PR$_1$gd**), drill hole no 15,195	graphite Q-biotite schists	up to 1.75	Velikanov et al., 2010
12	Novokryvorizka Suite **(AR$_3$nk)**, Ingul Block of the Ukrainian Shield, tectonic zone containing also U–Pb–Cu–Mo–Bi–Y minerals Red Miner deposit	silicified amphibole-magnetite quartzites and amphibol-bitite schists	up to 5.0, Ag- 50	Kalashnyk and Kuzmin, 2016
13	Novokryvorizka Suite **(AR$_3$nk)**, Mine	Quartz-albite veins	up to 11.3	Evtekhov et al., 1999

(continued on next page)

Table 2 (*continued*)

no	Geological unit, deposit	Rock type	Au [ppm]	References
	Kirovo			
14	Gdantsevska Suite (**PR$_1$gd**), drill hole 13663, Rodina Mine	altered graphite schists	up to 0.5	Velikanov et al., 2010
15	Gdantsevska Suite (**PR$_1$gd**), Oktajbrs'ka Mine	Quartz-carbonatite veins cut metaconglomerates	up to 3.0	Velikanov et al., 2010
16	Gdantsevska Suite (**PR$_1$gd**), Frunze Mine	altered conglomerates	up to 4.0	Velikanov et al., 2010
17	Saksaganska Suite (**PR$_1$sx**), and Gdantsevska Suite (**PR$_1$gd**), Ubilejna Mine	Sulphide- quartz veins in Ferruginous horizons	up to 5.0	Velikanov and Velikanova, 2007
18	Saksaganska Suite (**PR$_1$sx**), Velika Gleevatka deposit	waste from mineral dressing plant	up to 1.0	Kozin, 2014.
19	Saksaganska Suite (**PR$_1$sx**) and Gdantsevska Suite (**PR$_1$gd**), Gvardejska Mine	sulphide-quartz breccia in the Ferruginous horizons	up to 4.0	Velikanov and Velikanova, 2007
20	Gdantsevska Suite (**PR$_1$gd$_1$**), Pervomajske deposit drill hole 16,912	breccia and metasomatic rocks	up to 1.77	Velikanov et al., 2010
21	Saksaganska Suite (**PR$_1$sx**) and Gdantsevska Suite (**PR$_1$gd**), Ternovska Mine	sulphides zones in Ferruginous horizons	up to 6.4	Velikanov and Velikanova, 2007
22	Gdantsevska Suite (**PR$_1$gd**), Pervomajske deposit	brecciated silicified graphite schists	up to 3.0	Velikanov et al., 2010
23	Saksaganska Suite (**PR$_1$sx^{2s}**), Pervomajske deposit	II amphibole-magnetite-haematite horizon	up to 1.0, Ag – 150, Pd- 0.35, Pt- 0.08	Velikanov and Velikanova, 2007
24	Saksaganska Suite (**PR$_1$sx**), East Gannivka Strip	metasomatosis zones in Ferruginous horizons	up to 0.5	Velikanov and Velikanova, 2007
25	Saksaganska Suite (**PR$_1$sx**), Gannivske and Pervomajske deposits	waste from mineral dressing plant	up to 3.7	Kozin, 2014
26	Novokryvorizka Suite (**AR$_3$nk**), East Gannivka deposit	greisen zones in amphibolites	up to 2.0	Yushin et al., 2008
27	Novokryvorizka Suite (**AR$_3$nk**), Western Gannivka Strip	contact zone of Novokryvorizka S. and Demurin granite	up to 2.0, Mo- 0.05–0.27%	Sukach and Riazantseva, 2018
28	Ingul Block of the Ukrainian Shield (**AR$_2$in**), Petrovo deposit, NW Kryvyi Rih structure	graphite-biotite gneisses and its gossan	up to 0.4 Ag – 5.0	Kozin, 2014.

Py – pyrite; asp – arsenopyrite, cpy – chalcopyrite; MDB – Middle Dniper Block.

In the KR Basin, alluvial gold is also recognized. High concentration (1–14.5 ppm, Fig. 4, Table 2 no 7) was noted in Quaternary sandy clays rewashed and concentrated in alluvial sediments of Ingulets and Saksagan rivers and their tributaries.

6. Location of massive arsenopyrite occurrences in the Ingulets deposit

In the Ingulets deposit zones containing massive arsenopyrite bodies have been found at the −134 m mining level in the Proterozoic quartz-mica schists (phyllite) of the Skelevatska Suite (Fig. 5), a section with metasomatic alteration was uncovered (Fig. 6). The massive altered phyllite body is 20 m long and 5 m thick. It is composed of biotite, actinolite metasomatites and metasomatite quartzites. This body is located near the contact of phyllites with the talc horizon (it is at the contact of the Middle and the Upper Sub-suites of the Skelevatska Suite), and tectonic zone (Fig. 5, and Fig. 7). Arsenopyrite crystals are randomly distributed within the metasomatic altered phyllites (Fig. 8). Quartz veins (190°-200°/60°-80°) up to 35 cm thick (Fig. 9) which are cut by a low angle schistosity of phyllites from the top to the bottom of the phyllite horizon occur in this zone. In general, arsenopyrite bearing quartz veins are located within the zones of secondary silicification.

7. Methods

Microprobe analyses were carried out using JEOL SQ8200 at the Critical Elements Laboratories, Faculty of Geology, and Geophysics and Environmental Protection, AGH-UST, Krakow, Poland. The EMP was operated in the wavelength-dispersion mode at an accelerating voltage of 20 kV, and a probe current of 40 nA, with a focused beam diameter of 1 µm. The following standards and measurement were used: AgLα (100%), AuMα (100%), SbLα (Sb_2S_3), Fe, and SKα (FeS_2), PbMα (PbS), HgMα (HgS), CdLβ (CdS), CuKα (CuFeS2), ZnKα, (ZnS), BiMα (10%), AsLα (GaAs). The original Jeol ZAF procedures were used for a final correction of all the elements examined. Calculated statistical parameters like average content, standard deviation and coefficient of variability of quantitative EMP measurements helped in interpretation the data set.

Based on earlier published work indicating that the fluid conditions of sulphides and coexisting quartz are different (e.g. Burlinson et al., 2012), only massive sulphide samples were selected for Baro-acoustic decrepitation (BAD). It has been carried out in the laboratory of the Ivano-Franco University of Lviv. Two gram macroscopically separated pure sulphides were selected and used for analyses. This method was applied to determine formation temperatures of the massive sulphides, in which microscopic observations revealed the presence of numerous voids, probably after gas-fluid inclusions. The hand selected sulphide

Fig. 5. N-part of the Ingulets open pit, Au-Ag-As- showing.

Fig. 6. Slope of the Ingulets open pit, mining level −134 m, location with arsenopyrite showing (detailed picture from Fig. 5 – Au, Ag-,As point).

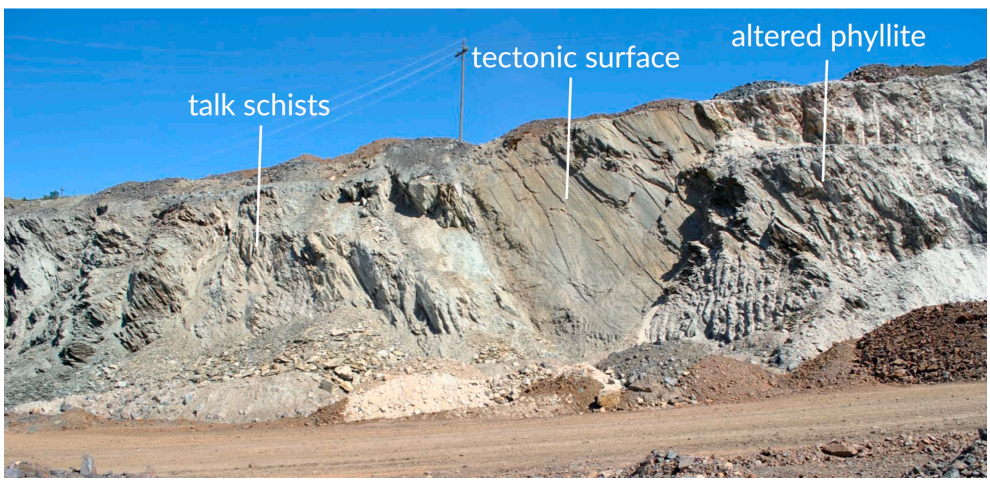

Fig. 7. Tectonic zone surface, −134 m mining level on the NE border of the Ingulets open pit.

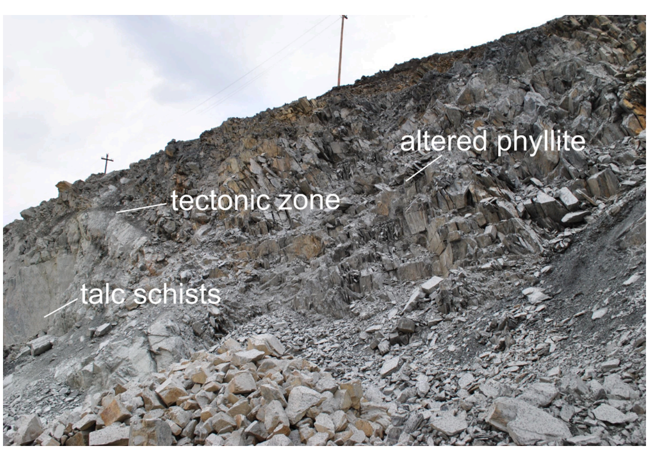

Fig. 8. Arsenopyrite occurrences locality at Ingulets, open pit, mining level −134 m.

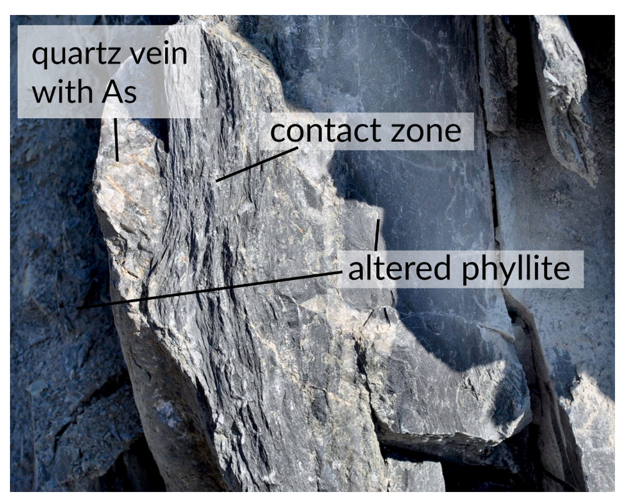

Fig. 9. Quartz vein in the metasomatic altered phyllite with arsenopyrite crystals.

material was crushed and sieved into a fine fraction of 200–420 μm (80–40 mesh). Such prepared samples were analysed with the BAG model 105[D1] Decrepitometre. The sieved sulphide samples were heated at a constant rate of 20 °C per minute from 100 °C to as high as 800 °C and as fluid inclusions generate high internal pressures they burst and can be detected with a pressure sensitive detector. Vacuum changes were simultaneously recorded digitally. The functions of decrepitometre were calibrated using standard samples. The arsenopyrite crystallization temperature was estimated based on the onset peak of the temperature. This point represents beginning of the decrepitation of inclusions. Decrepitation curve P(T) shows the pressure growth of gases, but the rate of decrepitation is described by derivative graph dP/dT(T).

Analyses of $\delta^{34}S$ were conducted in the Laboratory of Petroleum Geochemistry, Faculty of Geology, and Geophysics and Environmental Protection, AGH-University of Science and Technology (FGGEP, AGH-UST). The preparation of sulphur bound in sulphides (acid volatile sulphides) to Ag_2S was conducted using apparatus described by Mayer and Krouse (2004). Before reaction, the system was tested for the leakage, using nitrogen gas running 10 min. through the system. During the testing oxygen was removed from the system. The pulverised sample (ca. 0.5 g) was places in reaction flask and treated with 20% HCl as the reactor was heated in the nitrogen stream and constant temperature below the HCl boiling point (ca. 70 °C). Released H_2S with nitrogen was going through the trap with sodium citrate solution (2 wt%, pH = 4) and reacted with silver nitrate (0.1 M) forming Ag_2S. Solution with Ag_2S was filtrated, dried and delivered to the mass spectrometer Thermo Delta V Plus joined with elemental analyser Thermo Flash EA. Sulphur dioxide produced during A_2S burning in the elemental analyser was used for sulphur isotopes determination. The value of $\delta^{34}S$ is calculated as a ratio of $^{34}S/^{32}S_{sample\ minus}$ $^{34}S/^{32}S_{CDT\ and}$ $^{34}S/^{32}S_{CDT}$ (CDT is a standard based on iron meteorite from Diablo Canyon in Arizona). Accuracy of preparation and measurement was calculated on the level of ±0.2 ‰.

Bulk ICP-MS gold analyses were also performed in the Lab of the FGGEP, AGH-UST. Half of gram of a pure sulphide was dissolved using mixture of HCl (37%) and HNO3 (65%) (reversed Aqua regia) in ratio 1:3. The process was running 30 min in the MULTIWAVE 3000 (Anton Paar, USA) mineralizer at following conditions: temperature 230 °C, pressure 30 bar and 1200–1600 W. The obtained liquid was dissolved with pure water (18.2MΩcm) after culling. Analyses were carried out using spectrometer Elan 6100 (Perkin Elmer, USA).

8. Mineralogy and geochemistry of the polymetallic association

Several samples were investigated in reflected light microscope and both Electron microscope (EDS) and EMP measurements. Pyrite, arsenopyrite and tetrahedrite are the major minerals. Especially arsenopyrite forms vein type massive bodies and dispersions in the surrounding phyllite. Other minerals occur in much lower quantity.

8.1. *Pyrite, pyrrhotite*

Pyrite is a very common sulphide. It occurs in all ferruginous horizons forming dispersions and in all types of veins. In the ore horizons, it forms nests a couple of centimetres in size, laminae and vein type massive concentrations composed of both subhedral and euhedral crystals as well as irregular aggregates. Pyrite was found in quartz-arsenopyrite veins in some samples only, forming separate grains in association with arsenopyrite. Bulk ICP MS analyses of the vein type pyrite show gold concentration up to 4.26 ppm (sample Lz-2). It is probably refractory gold because gold grains were not found during microscopic investigation.

Pyrrhotite is common, associated with pyrite within the magnetite ores, however occurring in small quantity. It is a rare mineral within the metasomatic arsenopyrite zone and veins, and forms intergrowths with pyrite, arsenopyrite and occasionally inclusion in pyrite.

8.2. *Arsenopyrite*

In the KRIOB, arsenopyrite is generally classified as a very rare mineral. It mostly occurs in zones of hydrothermal mineralization together with minor pyrite, chalcopyrite and Ag-Sb- sulphosalts. Arsenopyrite from the central part of KRIOB (Ingulets deposit) is composed of: Fe–36.28%; As–43.45%; S–20.82%; SiO_2–0.06, and Au-0.12 ppm (bulk chemical analyses). Arsenopyrite occurrences are connected with high and middle temperature alteration and tectonic zones characterized by hydrothermal activity (Lazarenko et al., 1977).

Arsenopyrite is major mineral occurring in both quartz-arsenopyrite veins and surrounding altered host rock. It forms macroscopically massive concentrations with clearly visible crystals up to 2 cm in size, dispersed aggregates and well developed idiomorphic crystals up to 3–4 cm in size (Fig. 10A) in both quartz veins and metasomatically altered host rocks. Ore microscope investigation enabled recognition of two stages of arsenopyrite. The first stage is represented by coarse euhedral crystal of arsenopyrite (Figs. 10B, C, D and 11A, B, C, D). However, EMP-BSE images show internal crystal zoning (Fig. 10B, C). Differences in shadow visible in BSE images (Fig. 10B, C) result from variations in Ni and Bi concentration (Table 3, points 4, 6, 8, 12, 15, 16, 17, 20). It is suggested that crystal growth was completed simultaneously with some small changes in the fluid composition. The second stage of arsenopyrite is represented by small sized crystals (Fig. 11A) and aggregates (Fig. 11A) of massive sulphide and external rims (Fig. 11B, C) representing the second stage of hydrothermal activity. Arsenopyrite forms intergrowths with pyrite, pyrrhotite, tetrahedrite, sphalerite and chalcopyrite. It also contains inclusions of pyrite, pyrrhotite and minute gold grains (Fig. 10D).

Quantitative EMP measurements confirm their almost stoichiometric composition. Statistical parameters show low both standard deviation and coefficient of variability, of all analysed major elements, and high parameters on Ni (Table 3). The analysed arsenopyrite grains contain low admixtures of Sb–0.208 wt%, Ni–0.266 wt%, Co-0.07 wt% (all these are average values). Single points show also some elevated amounts of Ag, Bi and Au (Table 3). Statistical parameters show extremely high variability of Sb, Ni, Co and Bi and low variability of major constituents (Table 3). The highest concentration of Ni and Bi were measured in places characterized by zoning visible on BSE images (Fig. 10B, C, D).

8.3. *Tetrahedrite*

Tetrahedrite in quartz-arsenopyrite veins is the most common sulphide mineral. It forms small aggregates composed of differently oriented crystals (Fig. 12A, B, C, D). Usually it forms intergrowths with galena, sphalerite, (Fig. 13A), chalcopyrite, miargyrite (Fig. 13B, C, D), stibnite and sulfosalts (mostly miargyrite) (Figs. 13D and Fig. 14A, B, C, D). Ag, Ag-Pb and Pb sulfosalts are younger in relation to tetrahedrite (Fig. 13B). Zoning of tetrahedrites is quit visible on EMP-BSE images (Fig. 12A, B, C, D). It is a result of chemical compositional variability (Table 4). Outer zones are enriched in silver (Fig. 12A, e.g. points no 1, 2, 5, 7). In general, all analysed tetrahedrite occurrences are enriched in silver (Table 4). Based on EMP quantitative analysis three different groups were recognized. The first group is represented by typical tetrahedrite containing Ag on the level of 1,768 wt% to 5.123 wt% (Table 4). The silver content in the second group of tetrahedrite ranges between 8.267 wt% and 19.069 wt% (Table 4). A correlation plot of Cu-Ag (Fig. 15) show strong variance (R^2). It also explain high variability of silver content in mineralized solutions. All measured points represent tetrahedrite line however; Mozgova (1984, 2000) interprets variability in contents of other cations as a non-stoichiometric character of sulfosalts. High (−0.92324, for n = 40) correlation coefficient represents also Fe-Zn cations. Elevated amounts of iron show parallel decrease in Zn substitutions (Table 4).

Tetrahedrite with a Ag content above 27.675 wt% (Table 4, points 8, K-14, K-15) was assigned to the third group. High silver content in these grains enables classification of these phases as freibergite, which forms external rims and intergrowths with Ag-sulfosalts. The iron content in measured points is lower than 10 wt% and higher than in freibergite (3.47 wt% Fe). All point analyses also reveal elevated amounts of zinc, and some of them also elevated Bi, Cd, Hg and As (Table 4). Basic calculated statistical parameters show high variability of silver (86.22%), zinc (78.76%) and bismuth (107.69%), moderate of copper (22.05%) and iron (14.44%), and low of other basic constituent

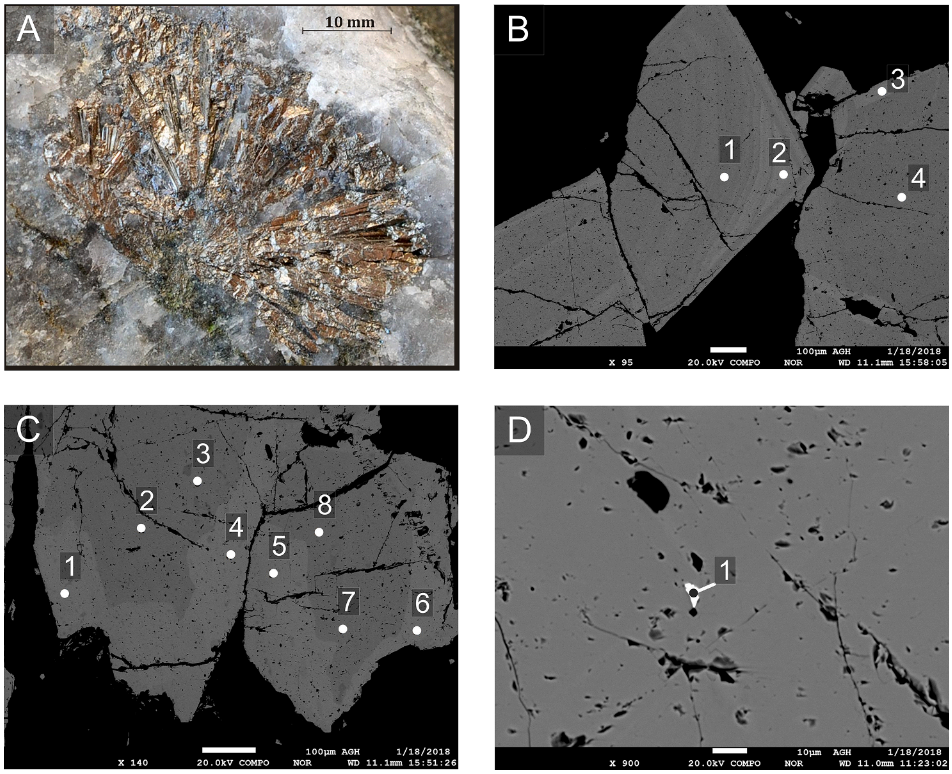

Fig. 10. A) Coarse arsenopyrite in quartz, Kryvyi Rih. B) Arsenopyrite crystals zoning, BSE image, 1–4 EMP points, sample KR2/5. C) Arsenopyrite crystal zoning. BSE image, 1–8 EMP points, sample Kr2/4. D) Gold grain (white) in arsenopyrite. BSE image, 1-EMP point, sample Kr2/3.

Table 3
EMP point composition of arsenopyrite in wt%.

No.	Sb Lα	Fe Kα	S Kα	Cu Kα	Ni Kα	Co Kα	Ag Lα	Bi Mα	As Lα	Au Mα	Total	Comment
1	2.350	34.146	20.193	0.439	n.d.	0.051	n.d.	0.090	43.656	n.d.	100.941	KR1 fot3-p8
2	0.056	34.501	19.482	0.881	0.095	0.151	n.d.	0.074	44.746	n.d.	99.986	KR1 fot10-p5
3	0.094	32.998	19.014	n.d.	0.305	0.217	n.d.	0.071	44.603	0.036	97.338	KR1 fot11-p1
4	0.122	34.962	19.548	n.d.	0.056	0.038	n.d.	0.085	43.686	n.d.	98.497	KR2 fo5-p1
5	0.094	34.734	19.753	n.d.	0.046	0.041	0.015	0.084	46.229	n.d.	100.996	KR2 fot1-p2
6	0.056	33.808	18.335	n.d.	0.472	0.043	n.d.	0.101	48.333	n.d.	101.141	KR2 fot1-p1
7	0.111	34.546	19.368	n.d.	0.081	0.069	n.d.	0.091	46.598	n.d.	100.890	KR2 fot1-p3
8	n.d.	33.852	18.254	n.d.	0.511	0.052	n.d.	0.103	48.154	n.d.	100.947	KR2 fot1-p4
9	0.055	33.763	18.632	n.d.	0.307	0.063	n.d.	0.091	47.734	0.043	100.688	KR2 fot2-p1
10	0.097	34.527	19.792	n.d.	0.051	0.049	n.d.	0.097	46.112	0.059	100.797	KR2 fot2-p2
11	0.059	34.373	18.930	n.d.	0.273	0.043	n.d.	0.076	47.662	n.d.	101.416	KR2 fot2-p3
12	0.047	33.435	17.966	n.d.	0.556	0.071	n.d.	0.060	48.325	n.d.	100.474	KR2 fot4-p1
13	0.201	34.770	20.016	n.d.	0.045	0.063	0.016	0.098	45.277	n.d.	100.484	KR2 fot4-p2
14	0.262	35.030	20.014	n.d.	0.032	0.056	n.d.	0.070	45.752	n.d.	101.220	KR2 fot4-p3
15	0.102	33.296	17.730	n.d.	0.908	0.075	n.d.	0.067	48.962	0.043	101.183	KR2 fot4-p4
16	0.073	33.720	18.210	n.d.	0.523	0.060	n.d.	0.021	47.773	n.d.	100.380	KR2 fot4-p5
17	n.d.	33.541	18.228	n.d.	0.525	0.063	n.d.	0.056	48.483	n.d.	100.896	KR2 fot4-p6
18	n.d.	34.764	19.789	n.d.	0.043	0.060	0.014	0.075	46.028	n.d.	100.774	KR2 fot4-p7
19	0.262	35.002	20.538	n.d.	0.037	0.070	n.d.	0.092	44.898	0.079	100.978	KR2 fot4-p8
20	0.064	33.700	18.336	n.d.	0.430	0.067	n.d.	0.086	48.481	n.d.	101.164	KR2 fot5-p2
	0.050	***0.033***	***0.022***	***0.026***	***0.030***	***0.035***	***0.015***	***0.021***	***0.185***	***0.036***		***detection limit***
Min.	0.013	32.998	17.730	0.439	0.032	0.038	0.015	0.021	43.656	0.036	97.338	
Max.	2.350	35.030	20.538	0.881	0.908	0.217	0.015	0.103	48.962	0.079	101.416	
Av.	0.208	34.173	19.106		0.266	0.070		0.079	46.575		100.566	
St.d.	0.509	0.624	0.846		0.255	0.042		0.019	1.709		0.983	
V [%]	244.71	1.82	4.42		95.86	60.00		24.05	3.67			n = 20

Av.- average; St.d. standard deviation; V- coefficient of variability; n.d.- not detected.

(Table 4). Copper reveals the highest variation among all major elements (Table 4). These variations could be explained by the substitution of copper by silver (Table 4). Calculated average atomic proportions (apfu) based on 13 S atoms are as follows: $(Cu,Fe,Zn,Ag)_{12.0855}Sb_{4.0017}S_{13.000}$ (Table 4). The typical formula of tetrahedrite is $(Cu_{9,7184}Fe_{1.9600}Zn_{0.0358},Ag_{0.2793})_{11.9935}Sb_{4.0853}S_{13.0000}$ (Table 4, point K-27). The calculated apfu formula for 16 cations of the highest Ag content minerals fits well to freibergite (Moëlo et al., 2008; Biagoni et al., 2020). It is as follows $(Ag_{5.9067}Cu_{4.2487}\text{-}Fe_{1.8672})_{12.0226}Sb_{3.9774}S_{11.7928}$ (Table 4, point K-14). The large differences in atomic proportions of cations can be explained by changes in chemical composition of the mineralizing fluids. Most of the measured

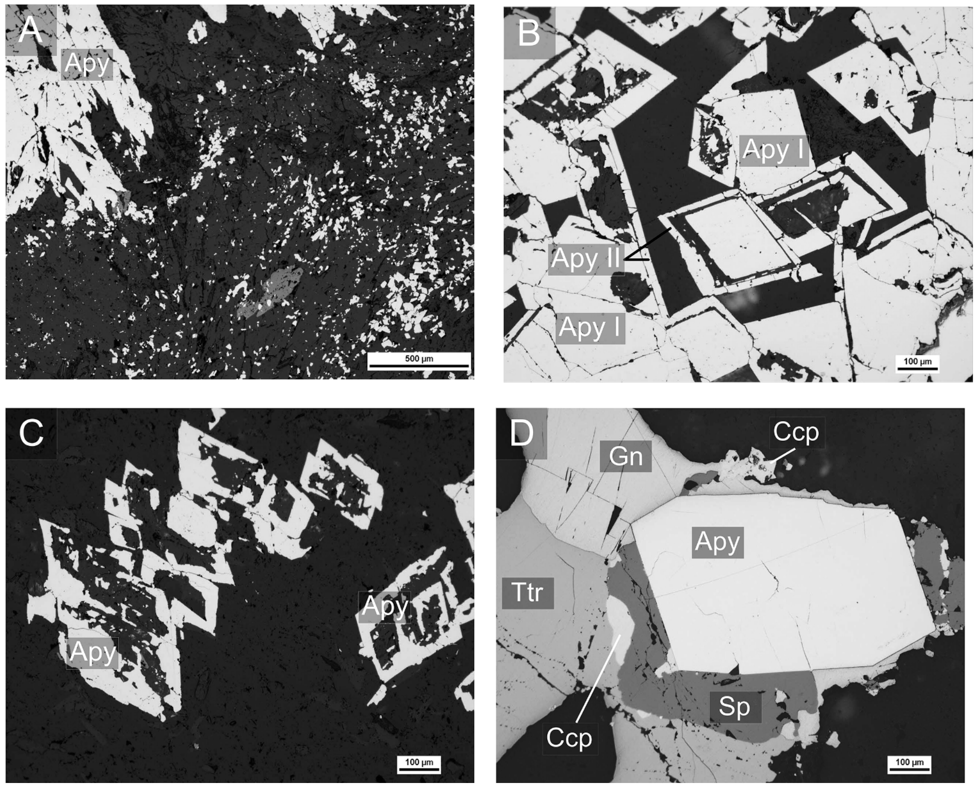

Fig. 11. Ore minerals in reflected light. A) Two stages of arsenopyrite (Apy), sample 6. B) Two stages of arsenopyrite (Apy), sample 2. C) Skeletal arsenopyrite (Apy) crystals, sample 8. D) Intergrowth of arsenopyrite (Apy) with sphalerite (Sp), chalcopyrite (Ccp), tetrahedrite (Ttr) and galena (Gn), sample 9.

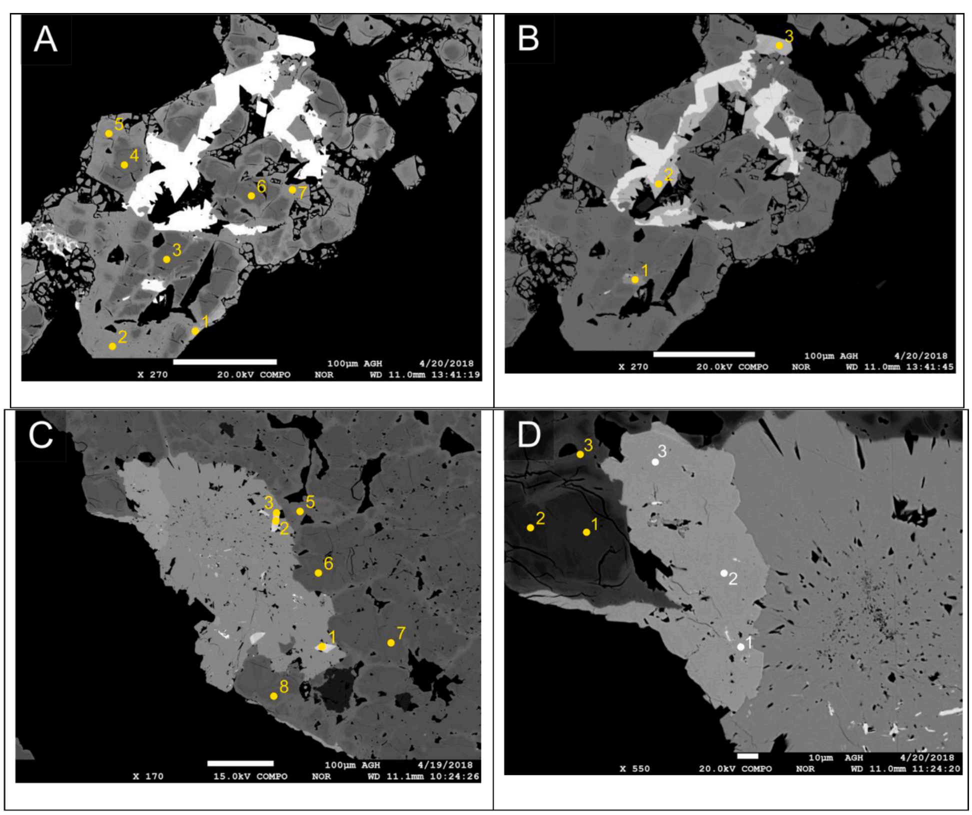

Fig. 12. A) Zoned tetrahedrite, white are Ag-Sb-sulfosalts, 1–7 EMP points, BSE image, sample AP459, fot. 10. B) Differences in Ag-sulfosalts, grey is tetrahedrite, BSE image, 1–3 EMP points, sample AP459 fot. 10. C) Zoned tetrahedrite, white are Ag-Sb-sulfosalts, 1–8 EMP points, BSE image, sample AP459 fot. 1. D) Zoned tetrahedrite, white are Ag-Sb-sulfosalts, 1–3 EMP points, BSE image, sample AP459, fot. 5.

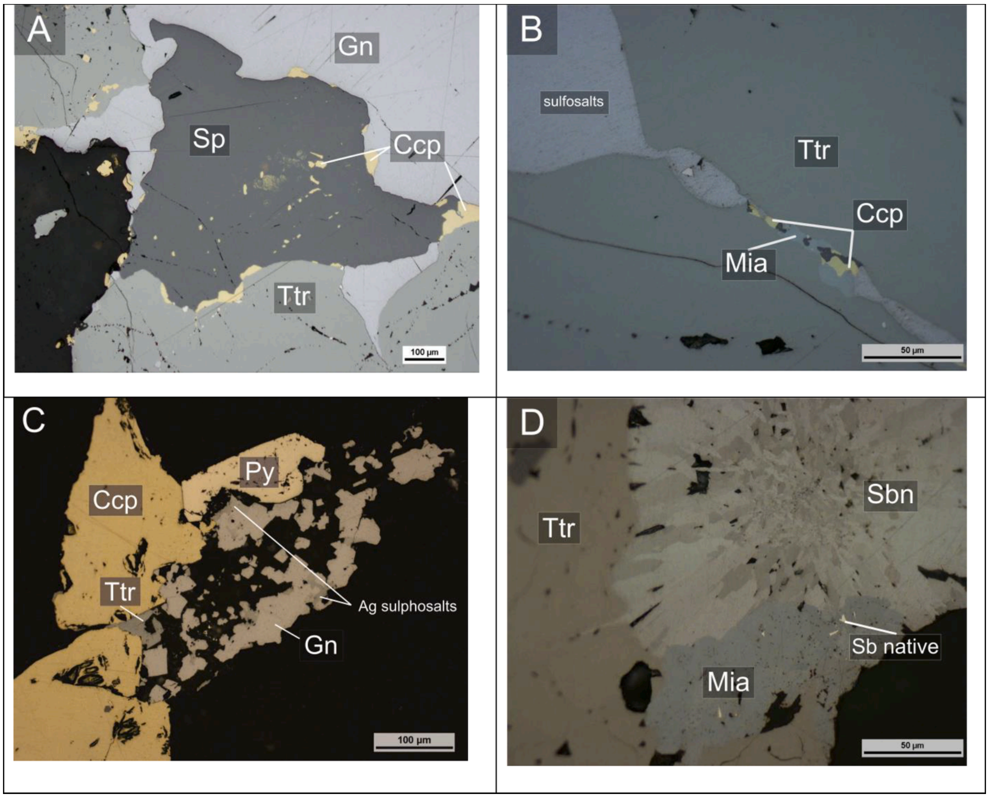

Fig. 13. Ore minerals in reflected light. A) Chalcopyrite (Ccp) inclusions in sphalerite (Sp), and tetrahedrite (Ttr), white is galena (Gn), sample 9. B) Chalcopyrite (Ccp), miargyrite (Mia) and Ag-Sb-sulfosalts association in tetrahedrite (Ttr), sample 9. C) Pyrite (Py), chalcopyrite (Ccp), tetrahedrite (Ttr) and Ag-sulfosalts association in quartz (black), sample 4. D) Intergrowth of stibnite (Sbn) with tetrahedrite (Ttr) and miargyrite (Mia) with small inclusions of Sb native (white), sample 4.

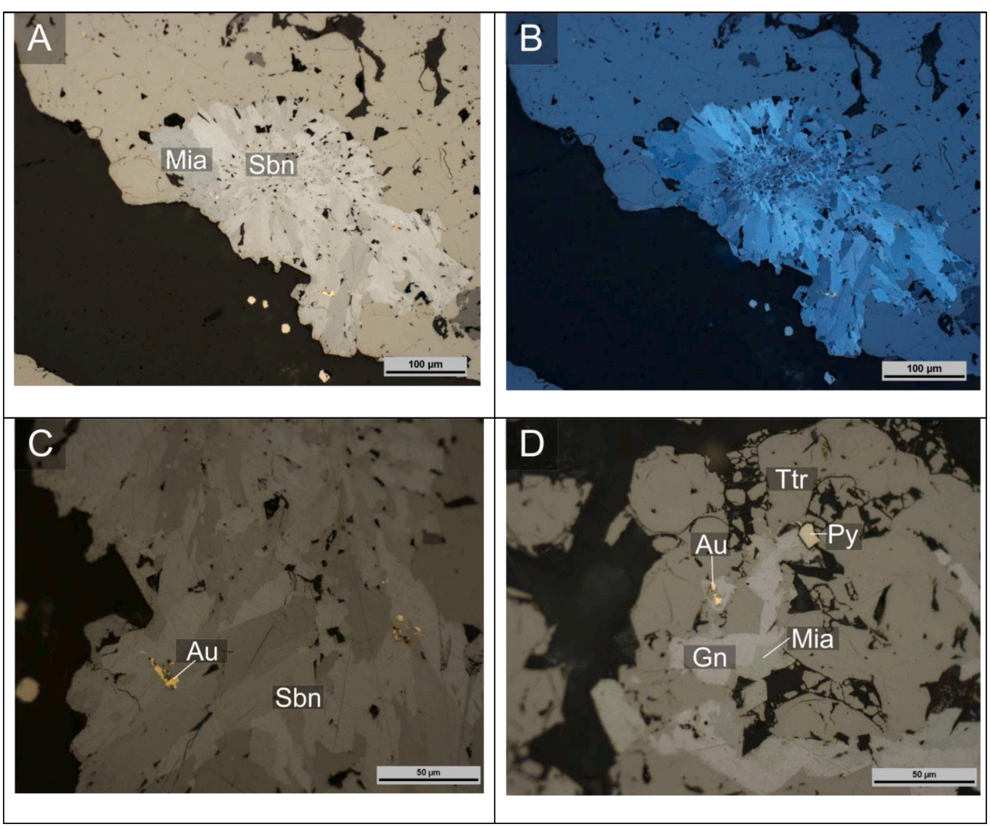

Fig. 14. Ore minerals in reflected light. A) Intergrowth of stibnite (Sbn) and miargyrite (Mia) with tetrahedrite (Ttr), sample 4. B) Intergrowth of stibnite and miargyrite with tetrahedrite, 70% crossed polars, sample 4. C) Gold (Au) inclusions in stibnite (Sbn), tetrahedrite – dark grey, sample 4. D) Gold (Au) inclusions in miargyrite (Mia), tetrahedrite (Ttr), Gn - galena, sample 4.

Table 4
EMP point composition of tetrahedrite in wt%.

No.	Ag Lα	Sb Lα	S Kα	Hg Mα	Cd Kα	Cu Kα	Zn Kα	Fe Kα	Bi Mα	As Lα	Total	Comment
1	8.267	28.627	24.309	n.d.	n.d.	32.590	0.014	6.366	0.029	n.d.	100.202	AP459 fot5-p1
2	5.123	28.975	24.605	0.042	n.d.	34.582	0.038	6.496	0.001	n.d.	99.862	AP459 fot5-p2
3	17.107	27.668	23.601	n.d.	n.d.	26.236	0.211	6.017	0.005	n.d.	100.845	AP459 fot5-p3
4	17.539	27.658	23.626	n.d.	n.d.	26.217	1.069	5.347	n.d.	n.d.	101.456	AP459 fot1-p5
5	2.990	29.200	24.792	n.d.	n.d.	35.956	2.216	4.564	0.006	n.d.	99.724	AP459 fot1-p6
6	3.197	28.678	24.416	n.d.	n.d.	35.747	2.262	4.554	n.d.	n.d.	98.854	AP459 fot1-p7
7	3.956	29.039	24.723	0.016	n.d.	35.529	0.939	5.771	0.001	n.d.	99.972	AP459 fot1-p8
8	27.675	26.915	21.766	n.d.	n.d.	18.726	0.021	5.979	n.d.	n.d.	101.082	AP459 fot9-p1
9	17.131	27.499	23.448	n.d.	n.d.	25.762	0.335	5.947	0.016	n.d.	100.138	AP459 fot9-p2
10	2.605	29.181	24.772	n.d.	0.029	36.324	2.707	4.134	0.006	n.d.	99.755	AP459 fot9-p3
11	6.357	28.880	24.386	0.008	n.d.	33.937	n.d.	6.591	0.010	n.d.	100.177	AP459 fot9-p4
12	16.756	27.401	23.175	0.058	n.d.	26.029	n.d.	6.240	0.006	n.d.	99.669	AP459 fot9-p5
13	4.452	28.866	24.841	n.d.	n.d.	35.328	0.670	6.065	n.d.	n.d.	100.222	AP459 fot9-p6
14	19.022	27.546	23.131	n.d.	n.d.	24.513	0.806	5.514	n.d.	n.d.	100.532	AP459 fot9-p7
15	17.725	27.432	23.403	0.015	n.d.	25.443	0.330	6.151	0.028	n.d.	100.527	AP459 fot6-p3
16	11.063	28.401	24.212	0.015	n.d.	30.501	1.986	4.525	0.045	n.d.	100.748	AP459 fot6-p4
17	3.859	28.961	24.677	n.d.	0.029	35.640	2.285	4.555	0.025	n.d.	100.029	AP459 fot6-p5
18	3.558	27.356	24.858	n.d.	n.d.	36.001	2.330	4.647	0.007	1.056	99.813	AP459 fot6-6
19	12.277	27.673	23.938	n.d.	n.d.	29.181	2.430	4.766	0.010	n.d.	100.275	AP459 fot6-p7
20	4.946	29.129	24.604	0.028	n.d.	34.875	2.059	4.724	n.d.	n.d.	100.365	AP459 fot6-p8
21	3.429	27.039	24.729	n.d.	0.039	36.211	2.892	4.139	n.d.	1.028	99.506	AP459 fot7-p3
22	4.862	29.013	24.598	n.d.	n.d.	34.819	2.333	4.547	n.d.	n.d.	100.172	AP459 fot7-p4
23	14.62	27.862	23.885	0.015	n.d.	27.964	1.239	5.279	n.d.	n.d.	100.864	AP459 fot7-p5
24	2.956	29.123	24.809	0.053	n.d.	35.938	2.468	4.417	0.041	n.d.	99.805	AP459 fot7-p6
25	2.459	28.002	24.943	n.a.	n.a.	37.594	n.d.	6.316	0.033	n.d.	99.916	Ap459 fot3-p3
K-25	2.610	27.490	24.519	0.021	n.d.	36.148	1.308	5.377	0.144	0.832	98.449	KR1 fot4-p2
K-26	3.019	27.532	24.428	n.d.	n.d.	35.892	1.184	5.344	0.144	0.813	98.410	KR1 fot4-p6
K-27	1.768	29.215	24.477	n.d.	n..d.	36.262	0.136	6.382	0.104	n.d.	98.347	KR1 fot6-p1
K-28	2.337	29.175	24.357	n.d.	n.d.	36.161	0.122	6.444	0.077	n.d.	98.673	KR1 fot6-p2
K-29	1.930	27.608	24.696	n.d.	n.d.	36.901	1.329	5.778	0.096	0.754	99.092	KR1 fot13-p1
K-30	1.888	27.724	24.682	n.d.	n.d.	36.512	2.801	4.059	0.097	0.665	98.432	KR1 fot15-p4
K-2	17.238	27.818	22.968	n.d.	n.d.	25.878	0.123	5.393	n.d.	n.d.	99.295	KR1 fot2-p2
K-9	2.811	27.686	24.628	n.d.	n.d.	36.136	1.374	5.565	0.046	0.848	97.720	KR1 fot4_p2
K-10	19.069	26.796	22.795	n.d.	n.a.	23.959	n.d.	5.963	n.d.	n.d.	98.582	KR1 fot.4-p3
K-11	18.512	27.108	22.854	n.d.	n.a.	24.640	n.d.	5.420	n.d.	n.d.	98.534	KR1 fot.4-p4
K-14	**33.813**	25.701	20.070	n.d.	n.a.	14.330	n.d.	5.535	n.d.	n.d.	99.449	KR1 fot.4-p8
K-15	**32.244**	25.830	20.415	n.d.	n.a.	14.808	n.d.	5.395	0.022	n.d.	98.710	KR1 fot.4-p9
K-16	4.267	27.154	24.404	n.d.	n.a.	35.319	0.543	7.163	0.031	0.746	99.086	KR1 fot9-p1
K-17	15.512	26.322	22.880	n.d.	n.a.	25.738	2.015	5.166	0.016	0.678	96.312	KR1 fot.12-p3
K-18	16.877	27.637	22.981	n.d.	n.a.	25.324	1.675	5.046	0.020	n.d.	97.941	KR1 fot.15-p4
	0.132	***0.087***	***0.021***	***0.015***	***0.028***	***0.026***	***0.021***	***0.033***	***0.043***	***0.055***		***detection limit***
Min	1.768	25.701	20.070	0.015	0.026	14.330	0.004	4.059	0.001	0.665	96.312	
Max	33.813	29.215	24.943	0.058	0.039	37.594	2.892	7.163	0.144	1.056	101.456	
Av.	10.196	27.923	23.885		0.031	30.616	1.229	5.442	0.039	0.824	99.539	
S.d.	8.791	0.951	1.142		0.007	6.354	0.968	0.786	0.042	0.139	1.048	
V [%]	86.22	3.41	4.78			20.75	78.76	14.44	107.69			n = 40

Co. Ni. Sn. In. Te. Se- sought but not detected (n.d.); n.a.- not analysed; Av.- average; S.d.- standard deviation; V- coefficient of variability.

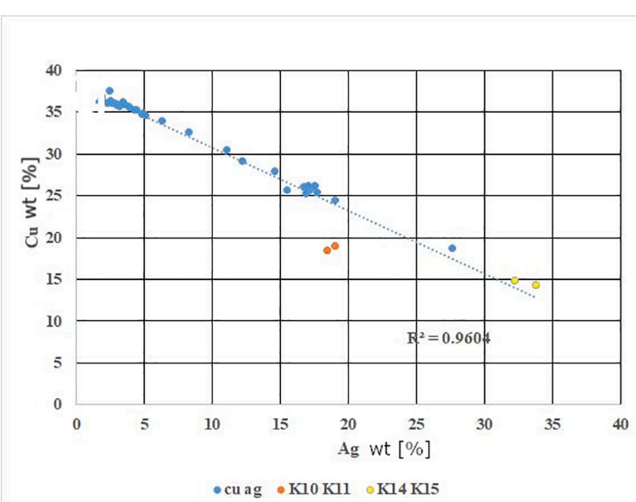

Fig. 15. Cu-Ag correlation plot in tetrahedrite.

grains contain no arsenic. Based on it, the distinct late stage of Ag-bearing association can be concluded.

8.4. Sphalerite

Sphalerite is a common mineral in quartz-arsenopyrite veins, however occurring in low quantities. It was found in several places within the KRIOB structure (Grechishnikov and Sakhatsky, 1973). It occurs in association with sulphides (Figs. 11D and 13A) and sulfosalts. It forms intergrowths with older sulphides like pyrite, arsenopyrite, tetrahedrite, chalcopyrite, and a younger association composed of galena and sulfosalts (Fig. 13A). Sphalerite grains comprise also irregularly distributed inclusions in chalcopyrite (Fig. 13A). EMP point measurements show high amounts of Cd admixtures and low content of other elements like Fe, Cu, Mn and Ge (Table 5). Lack of basinal brines, low content of Fe and high content of Cd suggests a deep source of hydrothermal fluids (Schwartz, 2000). The absence of silver suggest also early stage of crystallisation of sphalerite, probably simultaneous with chalcopyrite.

8.5. Chalcopyrite and galena

Chalcopyrite and galena, are common in the quartz-arsenopyrite

Table 5
EMP point composition of sphalerite, in wt%.

No.	S Kα	Fe Kα	Zn Kα	Cu K	Mn Kα	Cd Kα	Ge Lα	Total	Comment
1	32.388	2.427	61.084	0.038	0.017	3.086	n.d.	99.040	KR1 fot3-p6
2	32.571	2.289	62.128	0.037	0.030	2.584	n.d.	99.655	KR1 fot3-p7
3	32.319	2.729	60.462	0.089	0.047	3.587	n.d.	99.233	KR1 fot10-p2
4	31.897	2.698	61.001	0.056	0.044	3.034	0.052	98.785	KR1 fot10-p3
5	31.878	2.632	60.667	0.035	0.043	2.999	0.062	98.316	KR1 fot10-p4
6	32.612	2.468	61.799	0.315	0.028	2.219	0.033	99.474	KR1 fot15-p1
	0.014	***0.028***	***0.043***	***0.026***	***0.233***	***0.017***	***0.024***		***detection limit***
Min.	31.878	2.289	60.462	0.035	0.017	2.219	0.000	98.318	
Max.	32.612	2.729	62.128	0.315	0.047	3.587	0.062	99.655	
Av.	32.278	2.540	61.190	0.095	0.035	2.918	0.027	99.085	
S.d.	0.321	0.173	0.648	0.110	0.012	0.468	0.026	0.485	
V [%]	0.99	6.81	1.06	115.78	34.28	16.03			n = 6

Ag, Hg, In, Sn – sought but not detected (n.d.); Av.- average; S.d.- standard deviation; V- coefficient of variability.

veins. Both theses minerals form intergrowths with all other sulphides and sulfosalts (Fig. 11D and 13A, B C). Chalcopyrite forms also fine inclusions in sphalerite and tetrahedrite (Fig. 13A). EMP point analyses show stoichiometric composition of this mineral and a small admixture of gold up to 0.1 wt% in some points. Average composition based on 11 measurements show 33.909% Cu, 34.092% S and 30.32% Fe.

Galena is more common than chalcopyrite. Usually it forms small aggregates intergrown with Pb-Sb sulfosalts. EMP point measurements show its stoichiometric composition with small admixture of Bi, Cu, Fe, Te, and Ag. Measured points show relatively high amounts of Sb (Table 6). This is also confirmed by statistical parameters.

8.6. *Stibnite and Pb, Ag and Ag-Sb-Pb-sulfosalts*

Stibnite occurs in close association with all documented Sb-sulfosalts and also with tetrahedrite, chalcopyrite and galena (Figs. 13B, C, D and 14A, B, C), and native antimony. It forms intergrowths with all mentioned above minerals. Minute native Sb inclusions were identified in stibnite and miargyrite (e.g. Fig. 13D). Stibnite shows stoichiometric composition (Table 7). Stibnite contains 0.214 wt% of silver. Some EMP analytical points reveal small admixtures of silver (up to 0.214 wt%), copper (up to 0.160 wt%) and Bi (up to 0.126 wt%) (Table 7). Stibnite also forms mosaic type of intergrowth with Pb- and Ag-sulfosalts. Minerals of Sb- and Ag-sulfosalts group are difficult for ore microscope identification because of their similar optical properties like R, ΔR, colour, and hardness. All sulfosalts were identified using EMP quantitative point analyses (Table 8). Based on it zinkenite ($Pb_6Sb_{14}S_{27}$), plagonite ($Pb_5Sb_8S_{17}$), fuloppite ($Pb_3Sb_8S_{15}$), andorite ($PbAgSb_3S_6$) and chalcostibite ($CuSbS_2$) were identified (Tables 8, 10).

In the samples with Pb-sulfosalts Ag- and Ag-Cu sulfosalts have also been recognized. Miargyrite ($AgSbS_2$) is more common from this group and was identified using the ore microscope. It reveals stoichiometric composition (Table 9). Usually this mineral is characterized with a small admixture of Cu, up to 3.761 wt%, and Fe up to 1.865 wt% (Table 9). Other admixtures in miargyrite are negligible. Miargyrite forms intergrowths with chalcostibite and andorite. Both these minerals were identified based on EMP composition (Table 10)

8.7. *Native Au and Sb*

Gold was identified using bulk chemical analyses and optical and electron microscope investigation. The presence of gold was also confirmed by single bulk chemical ICP MS analyses. Massive pyrite shows 4,26 ppm Au (sample LZ-2) and massive, vein arsenopyrite −0.12 ppm Au. Optically visible gold was identified only in massive arsenopyrite samples containing nests of sulfosalts mineralization (Fig. 16). Gold forms minute size grains located in voids of arsenopyrite (Fig. 10A), stibnite (Fig. 14C), and miargyrite (Fig. 14D). It forms also thin (1 μm) veinlets splitting crystals of miargyrite (Fig. 16) which suggests a late stage of gold precipitation. Small size of gold grins and veinlets complicate precision of EMP analyses (Table 11). EMP analyses show electrum composition with small contamination by Sb, Bi and Hg.

Native Sb was recognized during EMP point checking (Fig. 12D). It occurs as small inclusions clearly visible also under the ore microscope (Fig. 13D). EMP point analyses show almost stoichiometric composition with some Bi, Cu, S and Ag contamination (Table 7) which is mostly due to small grain size.

Table 6
EMP point composition of galena in wt%.

No.	S Kα	Pb Mα	Bi Mα	Cu Kα	Fe Kα	Te Lα	Sb Lα	Ag Lα	Se Lα	Total	Comment
1	13.139	84.653	0.247	0.297	0.043	0.029	1.656	0.048	0.006	100.118	KR1 fot1-p1
5	13.048	85.274	0.159	0.211	0.008	0.059	1.464	n.d.	n.d.	100.224	KR1 fot1-p5
7	13.167	85.704	0.749	0.184	0.042	0.047	1.042	0.091	n.d.	101.026	KR1 fot5-p3
8	12.978	85.177	n.d.	0.185	0.025	0.084	1.087	0.051	n.d.	99.587	KR1 fot6-p1
9	13.052	87.470	0.659	0.054	0.029	0.053	0.615	0.008	n.d.	101.940	KR1 fot6-p2
10	13.148	83.490	0.816	0.232	0.031	0.027	1.489	0.058	n.d.	99.291	KR1 fot6-p3
16	13.020	85.867	0.960	0.081	0.079	0.066	0.552	0.051	n.d.	100.676	KR1 fot11-p3
18	13.105	85.383	1.028	0.394	0.163	0.040	1.138	0.058	0.011	101.320	KR1 fot12-p2
20	13.294	85.062	0.699	0.503	0.215	0.008	1.329	0.096	n.d.	101.206	KR1 fot15-p1
22	13.263	86.889	0.986	n.d.	0.044	0.039	0.631	0.095	n.d.	101.993	KR1 fot15-p3
	0.022	***0.132***	***0.063***	***0.071***	***0.035***	***0.037***	***0.087***	***0.132***	***0.128***		***detection limit***
Min.	12.978	83.490	0.159	0.046	0.008	0.008	0.552	0.008	0.000	99.291	
Max.	13.294	87.470	1.028	0.503	0.215	0.084	1.656	0.096	0.011	101.993	
Av.	13.121	85.497	0.700	0.219	0.068	0.045	1.100	0.062	0.004	100.738	
S.d.	0.102	1.111	0.311	0.148	0.067	0.022	0.395	0.028	0.005	0.927	
V [%]	0.77	1.29	44.42	70.47	98.52	48.88	35.90	45.16			n = 10

Au-sought but not detected; n.d.- not detected; Av.- average; S.d.- standard deviation; V-coefficient of variability.

Table 7
EMP point composition of stibnite and Sb-native in wt.%, Krivyi Rih.

No	SbLα	AgLα	SKα	PbMα	CuKα	FeKα	BiMα	SeLα	Total	Comment
3	71.435	0.214	28.153	n.d.	n.d.	0.026	n.d.	0.015	99,862	AP459_fot4_p5
4	71.384	0.162	28.218	n.d.	0.160	0.007	n.d.	n.d.	99.936	AP459_fot4_p6
8	71.402	0.115	28.290	n.d.	0.072	n.d.	n.d.	n.d.	98.879	AP459 fot1 p4
3	72.221	n.d.	27.759	n.d.	n.d.	0.017	0.075	n.d.	100.072	KR1_fot1_p3
4	71.211	n.d.	27.725	n.d.	n.d.	0.005	0.126	n.d.	99.067	KR1_fot1_p4
9	**92.923**	4.119	2.480	n.d.	0.083	0.010	0.053	n.d.	99.668	AP459_fot5_p1
19	**98.960**	n.d.	0.055	n.d.	1.194	0.531	0.650	n.d.	101.39	KR1_fot13_p2
6	**99.055**	n.d.	0.117	0.038	n.d.	0.066	0.056	n.d.	99.351	KR1_fot3_p5
	0.087	***0.112***	***0.022***	***0.028***	***0.071***	***0.035***	***0.053***	***0.128***		***detection limit***

Table 8
EMP point composition of Pb sulphosalts in wt%.

No.	Sb Lα	Ag Lα	S Kα	Pb Mα	Cu Kα	Fe Kα	Bi Mα	Se Lα	Total	Comment
1	44.776	n.d.	22.677	29.784	0.114	0.027	2.429	n.d.	99.807	AP459 fot4-p3 zinkenite
2	38.834	0.708	21.603	37.252	0.151	0.008	0.501	0.048	99.105	AP459 fot4-p4 plagonite
5	38.749	n.d.	21.431	39.699	0.129	n.d.	n.d.	0.068	100.076	AP459 fot1-p1 plagonite
6	41.544	0.107	21.929	33.055	0.252	0.018	3.193	n.d.	100.098	AP459 fot1-p2 zinkenite
7	38.404	n.d.	21.351	40.172	0.511	0.031	0.129	n.d.	100.598	AP459 fot1-p3 plagonit
10	38.840	n.d.	20.873	39.309	0.536	0.289	n.d.	0.002	99.849	AP459 fot3-p4 plagonit
11	46.832	0.022	22.940	29.726	0.399	0.216	n.d.	n.d.	100.135	AP459 fot3-p5 fuloppite
12	38.066	0.001	21.448	39.654	0.291	0.059	n.d.	n.d.	99.519	AP459 fot10-p2 plagonite
13	38.772	0.046	21.720	40.257	0.872	0.125	n.d.	n.d.	101.792	AP459 fot10-p3 plagonite
	0.087	***0.132***	***0.022***	***0.128***	***0.071***	***0.035***	***0.063***	***0.128***		***detection limit***

Te- sought but not detected, n.d.- not detected.

Table 9
EMP point composition of miargyrite in wt%.

No.	Sb Lα	Ag Lα	S Kα	Cu Kα	Bi Mα	Fe Kα	Se Lα	Pb Mα	Total	Comment
1	41.113	35.037	21.804	0.678	n.d.	0.019	n.d.	n.d.	98.651	Ap459 fot4-p7
2	41.286	36.498	22.004	0.555	0.102	0.026	n.d.	n.d.	100.471	Ap459 fot5-p2
3	41.227	36.017	22.267	0.753	n.d.	n.d.	0.011	n.d.	100.275	Ap459 fot5-p3
4	41.742	36.947	22.067	0.679	n.d.	0.025	n.d.	n.d.	101.460	Ap459 fot6-p1
5	41.504	36.004	22.058	0.798	0.323	0.016	n.d.	n.d.	100.703	Ap459 fot6-p2
6	41.861	36.247	21.964	0.379	n.d.	0.011	n.d.	n.d.	100.462	Ap459 fot7-p1
7	41.399	37.102	22.124	0.394	n.d.	0.012	n.d.	n.d.	101.031	Ap459 fot7-p2
8	41.856	37.094	21.792	1.021	n.d.	0.014	n.d.	n.d.	101.777	Ap459 fot8-p1
9	41.294	35.021	21.887	0.455	n.d.	0.006	n.d.	n.d.	98.663	Ap459 fot8-p2
10	39.901	35.965	22.421	2.527	0.011	1.865	n.d.	n.d.	102.690	Ap459 fot3-p1
13	42.269	35.962	21.899	1.788	n.d.	0.079	n.d.	n.d.	101.997	Ap459 fot10_p1
3	42.199	30.687	21.868	3.761	0.052	0.378	n.d.	n.d.	98.946	KR1 fot2-p3,
4	40.718	35.560	21.599	0.277	0.204	0.008	n.d.	0.434	98.800	KR1 fot5-p2
5	40.671	35.758	21.549	0.370	0.092	0.036	n.d.	0.858	99.334	KR1 fot5 p1
8	41.216	36.652	21.681	0.140	0.003	0.000	n.d.	n.d.	99.718	KR1 fot4-p1
12	41.205	36.078	21.510	0.270	n.d.	0.010	n.d.	n.d.	99.073	KR1 fot4-p5,
13	41.227	36.197	21.633	0.494	n.d.	0.049	n.d.	n.d.	99.600	KR1 fot4-p7
19	41.160	35.387	21.741	0.797	0.010	0.141	0.181Te	n.d.	99.470	KR1 fot15-p5
	0.087	***0.132***	***0.022***	***0.071***	***0.063***	***0.033***	***Te- 0.031***	***0.128***		***detection limit***

As-, Au- sought but not detected.

Table 10
EMP point composition of Sb-Cu and Ag-Sb-Pb, and Cu-Sb sulpho-antimonides in wt%.

No.	Sb Lα	Ag Lα	S Kα	Cu Kα	Bi Mα	Fe Kα	Pb Mα	Total	Comment
1	48.162	0.491	25.143	25.528	0.021	n.d.	n.d.	99.345	KR1 fot2-p1 chalkostibite
11	48.858	n.d.	25.728	26.440	n.d.	0.581	n.d.	99.916	Ap459 fot3-p2 chalcostibite
6	43.064	12.323	22.294	0.401	n.d.	0.140	24.647	102.869	KR1 fot5-p6 andorite
7	43.026	12.501	21.967	0.223	n.d.	0.050	25.042	102.825	KR1 fot5-p7 andorite
	0.087	***0.132***	***0.022***	***0.071***	***0.063***	***0.033***	***0.128***		***detection limit***

As-, Te- Se- sought but not detected; n.d.- not detected.

9. Discussion

It is a great challenge to start discussion on BIF and gold related deposits. First of all, these types of deposits were a subject of numerous publications (James, 1954; Gross, 1965 Kimberley, 1978; Simonson, 1985; Phillips et al., 1984; Groves et al., 1987; Klein, 2005). Classification is proposed based on different concepts e.g. mineral composition (James, 1954, tectonic setting (Gross, 1965), and depositional environment of iron facies (Kimberley, 1978; Simonson, 1985). Hamersley Basin in Australia, Kryvyi Rih in Ukraine, Kursk in Russia; Transvaal

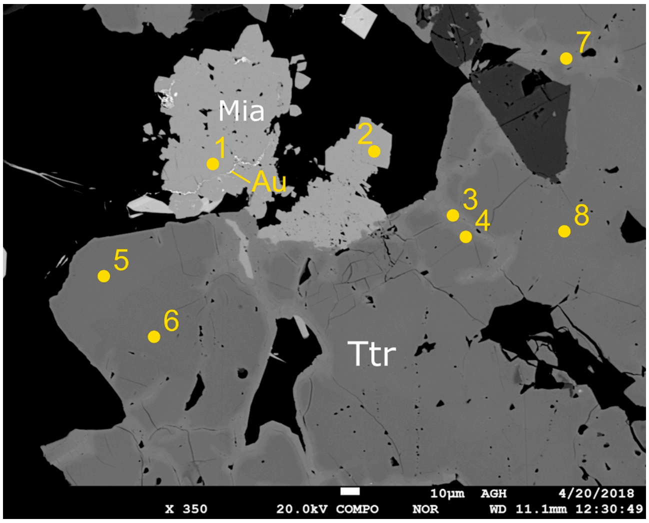

Fig. 16. Intergrowth of zoning tetrahedrite and miargyrite with minute size Au veinlets (white), BSE image; 1–8 – EMP point measurements. 459 fot 6.

Basin (South Africa), Labrador (Canada), Lake Superior in Canada and USA, Quadrilatero Ferrifero and Caue in Brazil (Robert et al., 2005; Pereira et al., 2007), and Singhbhum in India are the most important and characteristic representatives of the Superior type iron deposits (Woodall, 1979; Mukhopadhyay et al., 2008). From the economic point of view a large size (several hundred sq kilometers) and enormous volume of reserves are distinct features of these deposits. Apart from major constituents these deposits contain also some sulphides e.g. pyrite, and pyrrhotite which are also a subject of detailed genetic discussions – syngenetic (Fripp, 1976) versus epigenetic (Phillips et al., 1984; Groves et al., 1987). The huge size of these deposits makes an additional challenge for geologists thinking seriously on representative number and size of samples collected for investigation.

The Superior BIF type deposits are not only interesting because of huge tonnage of iron ores but also because of hosting gold and sometimes even Pd mineralization e.g. the Caue Iron deposit, Itabira District in Brazil (Olivo et al., 1995). Some occurrences of Au, Pd (0.35 ppm) are reported also from Pervomaysk deposit (Table 2) (Velikanov and Velikanova, 2007). In the case of KR, arsenopyrite, marcasite, chalcopyrite, sphalerite, and galena are also documented (Lazarenko et al., 1977; Sośnicka et al., 2015).

In the KR basin 28 location containing gold have been identified (Table 2). In the middle zone of the Skelevatska Suite (Figs. 1, 2), an unusual mineral association is described. Apart from iron ore stage, three other stages of polymetallic mineralization are documented (Table 12). The first stage is high temperature of a hydrothermal alteration. Silicification and epidotisation with minor pyrite and arsenopyrite result from high temperature fluids following the younger tectonic system. The second stage is composed of base metals sulphides (Table 12). Decrepitation patterns show three zones with of pressure changes. The first zone is dedicated to the secondary inclusions in the temperature range 100–150 °C. In the second one, temperature of the decrepitation of inclusions in arsenopyrite begins at 450 °C and ends at 650 °C (Fig. 17). It can be interpreted that this stage was related also to the host rock alteration, which began at 450 °C and ended at 650 °C. This fact is also confirmed by the dispersions of arsenopyrite within the zone of host rock alteration. The maximum peak of decrepitation is about 585 °C. It might be related to the second alteration episode affecting the iron ores described by Sośnicka et al. (2015). It fits well with the stability field of arsenopyrite (Sharp et al., 1985; Tomkis et al., 2006). In general, arsenopyrite forms zoned crystals (Fig. 10B, C), which

Table 11
EMP point composition of electrum in wt.%,

No.	Sb Kα	Ag Lα	Hg Mα	Pb Mα	Fe Kα	Au Lα	Bi Mα	Cu Kα	Total	Comment
1	0.976	20.244	0.067	n.d.	n.d.	79.817	0.073	0.006	101.183	Ap459 fot4-p1
2	0.359	20.670	0.020	n.d.	n.d.	80.305	0.117	n.d.	101.471	Ap459 fot4-p2
3	0.524	33.335	0.349	0.747	0.021	67.089	0.072	0.17	103.207	Ap459 fot2-p1
4	n.d.	10.644	1.131	n.d.	9.139	77.333	0.491	n.d.	102.627	KR2 fot3-p1

n.d.- not detected; As-sought but not detected.

Table 12
Mineral succession and stages of mineralization.

Minerals	Iron ore stage	Stage I (host rock alteration)	Stage II	Stage III
garnet	———			
cummingtonite	==========	————		
chlorite	————————	———————		
biotite	——————————————			
magnetite	==========	————————		
hematite	======	======		
ilmenite	–			
graphite	–			
epidote		——————		
quartz		—————————————————	——————————————	
arsenopyrite		?	—————————————————I	—————II
pyrite	–	—	———	—
pyrrhotite			———	
tetrahedrite			——— I	———— II
sphalerite			———	
chalcopyrite			———	
galena				—
Sb-native				–
stibnite				——
miargyrite				—
gold				–
other sulfosalts				————
carbonates				——

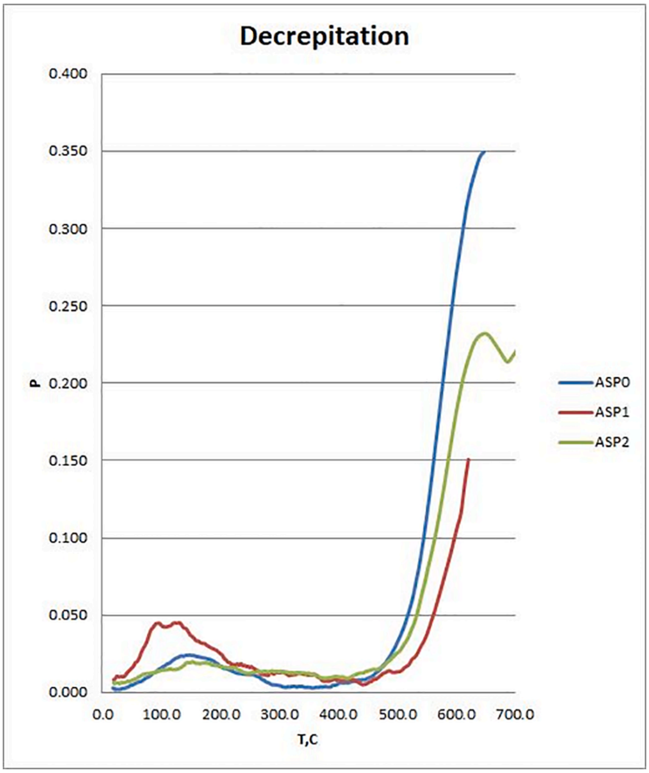

Fig. 17. Decrepitation curves of arsenopyrite and pyrite.

have been classified into separate stages (Table 12). It is probable the zonning results in the wide range of the decrepitation temperature showing on Fig. 17. The fluids enriched in Sb represented mostly by tetrahedrite (Table 2) also characterize this stage. The third stage is characterized by a broad composition of various Ag-Pb-Cu sulfosalts (Tables 8, 9, 10 and 12) and stibnite (Table 7). Native Sb and electrum appears at the end of the third stage fluids activity.

Two different sulphide assemblages were selected for sulphur isotopes measurements. Arsenopyrite was selected from the massive bodies containing also polymetallic mineralization, therefore pyrite was collected from massive stratiform concentration related to magnetite ores. Both these minerals show different $\delta^{34}S$ composition (Table 13), which confirms two sources of the sulphur. Arsenopyrite sulphur isotopes $\delta^{34}S$ show small variability (Table 13). The positive values are characteristic for the fluids having connection with a deep magmatic source (Sakai, 1968; Ohmoto, 1972; Allard, 1983; Taylor, 1986; Poorter et al., 1991; Ridley and Diamond, 2000; Hoefs, 2009). Similar value of the $\delta^{34}S$ (0.7–1.0‰) are reported by Sakai et al., (1982) in the Kiluauea gases and 0.9–2.6‰ for Mount Etna (Allard, 1983) and in the gold mineralization from the BIF formation in the Amalia greenstone belt deposit (Adomako-Ansah et al., 2013). Sulphur isotopes of pyrites are different from those measured on arsenopyrites (Table 12).

Table 13
Sulphur isotopes in arsenopyrites and pyrites.

Kryvyi Rih	Mineral	$\delta^{34}S$	Locality
KR-1	arsenopyrite	1.2	Ingulec GOK
KR-2	arsenopyrite	0.6	Ingulec GOK
KR-3	arsenopyrite	1.1	Ingulec GOK
KR-2p	arsenopyrite	1.1	Ingulec GOK
KR-6p	arsenopyrite	0.9	Ingulec GOK
KR-7p	arsenopyrite	1.3	Ingulec GOK
Łz-1	pyrite	−6.2	Central GOK
Łz-2	pyrite	−3.0	Central GOK
IGOK-1	pyrite	−2.7	Ingulec GOK
IGOK-2	pyrite	−3.2	Ingulec GOK

Heterogeneity of $\delta^{34}S$ in pyrites can also be variable due to the distance between places of crystallization and geotectonic position (Hoefs, 2009). It can be also explained by a different stage of pyrite crystallization, which took place prior to the arsenopyrite. Therefore Hoefs (2009) suggests possible contamination during stratiform sedimentation and later instable balance of temperature and related H_2S content and water fugacity. Therefore, pyrite samples were collected from texturally different localities and ore horizons. No replacement of iron oxides are observed in the massive arsenopyrite body.

10. Summary

In general gold-bearing BIF deposit are less common than classic greenstones-hosted ones (Goldfarb, et al., 2005) however association of gold and BIF iron-type deposits is known worldwide (Pereira et al., 2007; Fyon et al., 1983; Armitage et al., 1996; Vielreicher et al., 1994; Gilligan and Foster, 1987; Groves and Foster, 1991; Castro, 1994). The following deposits represent good examples: Sao Bento Gold (Lobato et al., 1998; Lobato et al., 2001), Cuiabá (Ribeiro-Rodrigues et al., 2000) and Raposos (Junqueira et al., 2007). Other similar types of deposit (Muselwhite in Ontario and Meadowbank in Nunavut) are known from Canada (Fyon et al., 1983, Armitage et al., 1996; Castonguay et al., 2015). Epigenetic gold mineralization is usually related to pyrrhotite replacing magnetite (Robert et al., 2007) according to the following equation $2Fe_3O_4 + 3HAu(HS)_2 = 6FeS + 3Au + 9/2H_2O + 7/4O_2$ (Phillips et al., 1984).

Gold is widespread within the whole productive KR Basin, that is 130 km long, and is also reported from several points located within the metacoglomerates (2.6 Ga) occurring below the talc horizon. KR Basin is characterized by massive, metasomatic iron ore bodies, which are controlled by the younger faults (Fig. 6) and occurring only in places with the talc horizon in the footwall (Belevcev, 1973; Pieczonka et al., 2011; Sośnicka et al., 2015). Gold content in the silicified zones of the fresh metaconglomerate reach 1.2 ppm (Pieczonka et al., 2011) and in altered metaconglomerate 4 ppm e.g. at Frunze Mine (Velikanov Y.F. et al., 2010, see also Table 2). The role of the enormous mass of magnetite hematite ore on gold concentrations is difficult to assess. Presence of gold traces in both i) all feruginous horizons and ii) methasomatic zones related to the tectonic structures located within different lithological units, not confirmed such a hipothesis. Firstly, it is documented by the bulk chemical analyses of the waste samples containing economic grade of gold, collected in mineral enrichment plants (Table 2, point no. 5). However gold was also dicoverd within the other surrounding suits eg. in metaconglomerate of the Skelevatska Suit or in breccia related to the tectonic zones at Kryvyi Rih Series (compare also Table 2 point 29). Localization of gold concentration within the different geological environment and sulphur isotopes confirm ~~rather~~ hydrothermal hypothesis. The number of the gold showing within the KR basins is a good prognosis for further exploration. It confirms wide dispersion of gold not only in the altered tectonic related section but also within the widely distributed iron ore bodies. Association of gold with arsenopyrite and Ag-Sb sulfosalts is for the first time described in the KR basin. With reference to the thick hydrothermal and structurally controlled altered zone and the high temperature of mineral assemblage mesothermal type and deep source of fluids might be concluded (Groves et al., 2003, Goldfarb et al., 2005). Discussion on the gold-polymetallic mineralization open a new field for further exploration of well-known BIF related deposit.

CRediT authorship contribution statement

Anatolyi Berezovsky: Resource, Investigation. **Jadwiga Pieczonka:** Investigation. **Adam Piestrzynski:** Supervision, Writing - review & editing.

Declaration of Competing Interest

The authors declare that they have no known competing financial interests or personal relationships that could have appeared to influence the work reported in this paper.

Acknowledgements

Acknowledgement are going to the Faculty of Geology, Geophysics and Environmental Protection, AGH-UST Krakow for the continual financial support Grant AGH 16.16.140.315). We thank G. Kozub for EMP measurements and T. Ćwiertnia for making graphic. We are thankful to Marek Wendorff for useful discussion, and John Clifford for English improving. The authors also want to thank the anonymous reviewers for their work and help.

References

Adomako-Ansah, K., Mizuta, T., Hamond, N.Q., Ishiyama, D., Ogata, T., Chiba, H., 2013. Gold mineralization in banded iron formation in theAmalia Greenstone Belt, South Africa: a mineralogical and sulfur isotope study. Resour. Geol. 63 (2), 119–140. https://doi.org/10.1111/rge.12000.

Allard, P., 1983. The origin of hydrogen, carbon, sulphur, nitrogen and rare gases in volcanic exhalations: evidence from isotope geochemistry. In: Tazieff, H., Sabroux, J. S. (Eds.), Forecasting Volcanic Events. Elsevier, Amsterdam, pp. 337–386.

Armitage, A.E., James, R.S., Goof, S.R., 1996. Gold mineralization in Archean banded iron formation, Third Portage Lake area, Northwest Territories, Canada. Explor. Min. Geol. 5, 1–15.

Belevcev, Y.N., 1973. Genesis of high-grade iron ores of Kryvyi Rich type. In: Genesis of Precambrian Iron and Manganese Deposits, Proceedings of the Kiev Symposium, August 1970. UN Educational Scientific and Cultural Organization, Paris, 167-180.

Belevcev, Y.N., Toxtev, G.V., Strihin, A.I., 1962. Geology of iron deposits Kryvyi Rich, Kiev. Acad. Sci. SU 1. C, 1–484.

Belevcev, Y.N., Epatko, J.M., Werigin, M.I., 1981. Ukrainian Precambrian iron deposits and their prognosis and economy. Naukova Dumka, pp. 230, (in Ukrainian).

Biagoni, C., Luke, L., George, Cook, N.J., Makovicky, E., Moëlo, Y., Pasero, M., Sejkora, J., Stanley, C.J., Welch, M.D., Bosi, F., 2020. The tetrahedrite group: Nomenclature and classification. Am. Mineralogist 105, 109–122.

Burlinson, K., Mernagh, T., Gaboury, D., Jiuhua Xu, LonghuaLin, 2012. Fluid Inclusion Studies on Opaque minerals ACROFI-4 Conference, Brisbane Qld., August 2012 www.appliedminex.com/decrep/orals/bne12/opaquedecrep.htm.

Castonguay, S., Dube B., Mercier-Langevin P., McNicoll V., Oswald W., Janvier V., Malo, M., 2015. Geological controls of BIF-hosted gold mineralization: Insights from the World-class Musselwhite (Ontario) and Meadowbank (Nunavut) deposit, Canada. In: Mineral resources in a sustainable world, Proceeding book, 13 SGA Meeting, Nancy-France V3, 1067-1070, DOI:10.13140/RG.2.1.1224.6246.

Castro, L.O., 1994. Genesis of banded iron formations. Econ. Geol. 89, 1384–1397.

Fripp, R.E.P., 1976. Stratabound gold deposits in Archaean BIF, Rhodesia. Econ. Geol. 71, 58–75.

Evtekhov, V.D., Paranko, I.S., Evtekhov, E.V., 1999. Alternative Resource Base of Krivoy Rog Iron-Ore Basin. Krivoy Rog Technical University Press, p. 70 (in Russian).

Fyon, J.A., Crocket, J.H., Schwarcz, H.P., 1983. The Carshaw and Malga iron-formation-hosted gold deposits of the Timmins area. In: Colvine, A.C. (ed.), The Geology of Gold in Ontario. Ontario Geological Survey Miscellaneous Paper 110, pp. 98–110.

Gilligan, J.M., Foster, R.P., 1987. Gold mineralization in iron-formation: the importance of contrasting modes of deformation at the Lennox Mine, Zimbabwe. In African Mining. Inst. of Mining and Metallurgy, London, 127–138.

Goldfarb, R.J., Baker, T., Dubé, B., Groves, D.I., Hart, C.J.R., Gosselin, P., 2005. Distribution, Character, and Genesis of Gold Deposits in Metamorphic Terranes. In: Hedenquist, J.W., Thompson, J.F.H., Goldfarb, R.J., Richards, J.P. (eds.) Economic Geology 100th Anniversary Volume, 407-450.

Grechishnikov, N.P., Sakhatsky, I.I., 1973. To the question of the conditions of gold accumulation in Krivoy Rog conglomerates. Geol. J. 33 (3), 110–113 (in Russian).

Gross, G.A., 1965. Principal Types of Iron-Formation and Derived Ores. Annual General Meeting. Toronto. Transactions VLXIX, 41-44.

Groves, D.I., Foster, R.P., 1991. Archaean lode gold deposits. Gold Metallogeny and Exploration. Springer, Boston, MA https://doi.org/10.1007/978-1-4613-0497-5-3.

Groves, D.I., Phillips, G.N., Ho, S.E., Houstoun, S.M., Standing, C.A., 1987. Craton-scale distribution of Archaean greenstone gold deposits: predictive capacity of the metamorphic model. Econ. Geol. 82, 2045–2058.

Groves, D.I., Goldfarb, R.J., Robert, F., Hart, C.J.R., 2003. Gold Deposits in metamorphic belts: overview of current understanding, outstanding problems, future research, and exploration significance. Econ. Geol. 98 (1), 1–29.

Gurskiy, D.S., (ed) + 61 co-authors, 2002. Main types of rock complexes and mineral deposits in the Ukrainian Shield, Geological excursion guidebook. Mtallogeny of Precambrian Shilds. Kyiv 2002, Ukrainian State Geological Survey, BLITZ PRINT Kyiv, pp. 166.

Hoefs, J., 2009. **S**table isotope geochemistry-Hoefs. Springer 1–281.

James, H.L., 1954. Sedimentary facies of iron-formation. Econ. Geol. 49, 235–293.

Junqueira, P.A., Lobato, L.M., Ladeira, E.A., Simões, E.J.M., 2007. Structural control and hydrothermal alteration at the BIF-hosted Raposos lode-gold deposit, Quadrilátero Ferrífero, Brazil. Ore Geol. Rev. 32 (3-4), 629–650. https://doi.org/10.1016/j.oregeorev.2006.03.004.

Kalashnyk, G.A., Kuzmin, A.V., 2016. Preconditions of formation and criteria for prognostication of copper-uranium ore-formation in West-Inguletstka fault zone of the Ukrainian shield. Zbirnyk naukovykh prats UkrDHRI 2. P., 61-81, (in Russian).

Kimberley, M.M., 1978. Paleoenvironmental classification of iron formation. Econ. Geol. 1973, 215–229.

Klein, C., 2005. Some Precambrian banded iron-formations (BIFs) from around the world: Their age, geologic setting, mineralogy, metamorphism, geochemistry, and origins. Am. Mineralogist 90 (10), 1473–1499. https://doi.org/10.2138/am.2005.1871.

Kozin, L.F., 2014. Chemistry and technology of noble metals - gold and silver. Problems and prospects. Kiev, Interservice 1, pp. 744 (in Russian).

Kulish, E.A., Gurskiy, D.S., 2005. Black metals - Iron. In: Szczerbak, M.P., Bobrow, A.B. (eds.), Metalliferous and non-metal deposits of Ukraine vol. 1, 59-106 (in Russian).

Latys, I.K., Shaposhnikov, V.A., 1974. Geochemistry of impurity elements of the Skelevatsky Magnetite deposit. Publishing House "Naukova Dumka". Kiev, pp. 64, (in Russian).

Lazarenko, E.K., Gershoyg, Yu.G., Buchinskaya, N.I., 1977. Mineralogy of the Kryvyi Rih basin. Kiev, Naukova Dumka , pp. 1-544, (in Russian).

Lobato, L.M., Ribeiro-Rodrigues, L.C., Vieira, F.W.R., 2001. Brazil's premier gold province: Part II: geology and genesis of gold deposits in the Archean Rio das Velhas greenstone belt Quadrilátero Ferrífero. Miner. Deposita 36 (3-4), 249–277.

Lobato, L.M., Vieira, F.W.R., Ribeiro-Rodrigues, L.C., Pereira, L.M., Menezes, M.G., Junqueira, P.A., Pereira, S.L., 1998. Styles of hydrothermal alteration and gold mineralization associated with the Nova Lima Group, Quadrilátero Ferrífero: part II, the Archean mesothermal gold-bearing hydrothermal system. Braz. J. Geol. 28, 355–366.

Machado, O.T., Yurtaeva, A.D., 1997. Gold content of magnetite-silicate quartzites of the southern part of the Inguletsky deposit. Vedomosti of the Academy of Mining Sciences of Ukraine 4. P., 110-111, (in Russian).

Mayer, B., Krouse, H.R., 2004. Procedures for sulphur isotope abundance studies. In: de Groot P.A. (ed.), Handbook of Stable Isotope Analytical Techniques 1, B.V. Elsevier, 538 – 596.

Metchnikov, J.P., 2000. About some important aspects of gold prospecting in Kryvyi Rih. Geol. Mineral. Bull. 1-2, C., 48-51 (in Russian).

Moëlo, Y., Makovicky, E., Mozgova, N.N., Jambor, J.L., Cook, N., Pring, A., Paar, W., Nickel, E.H., Graeser, S., Karup-Møller, S., Balic-Žunic, T., Mumme, W.G., Vurro, F., Topa, D., Bindi, L., Bente, K., Shimizu, M., 2008. Sulfosalt systematics: a review. Report of the sulfosalt sub-committee of the IMA Commission on Ore Mineralogy. Eur. J. Mineral. 20 (1), 7–46.

Mozgova, N.N., 1984. Prinicples of classification of sulfosalts. In: Proceedings of 27th International Congres, Moscow, Section C10, 53-65.

Mozgova, N.N., 2000. Sulfolsalts mineralogy today. In: IMA COM Short Course: Modern Approaches to Ore and Environmental Mineralogy. Espoo, Finland, p. 4.

Mukhopadhyay, J., Gutzmer, J., Beukes, N.J., Bhattacharya, H.N., 2008. Geology and genesis of the major banded iron formation-hosted high-grade iron ore deposits of India. Rev. Econ. Geol. 15, 291–316.

Ohmoto, H., 1972. Systematic of sulfur and carbon isotopes in hydrothermal ore deposit. Econ. Geol. 67, 551–578.

Olivo, G.R., Gauthier, M., Bardoux, M., Lea De Sa, E., Fonseca, J.T.F., Santana, C., 1995. Palladium-Bearing Gold Deposit Hosted by Proterozoic Lake Superior-Type Iron-Formation at the Caue Iron Mine, Itabira District, Southern Sao Francisco Craton, Brazil: Geologic and Structural Controls. Economic Geology 90, 118-134.

Pereira, S.L.M., Lobato, L.M., Ferreira, J.E., Jardim, E.C., 2007. Nature and origin of the BIF-hosted São Bento gold deposit, Quadrilátero Ferrífero, Brazil, with special emphasis on structural controls. Ore Geol. Rev. 32 (3-4), 571–595.

Phillips, G.N., Groves, D.I., Martyn, J.G., 1984. An epigenetic origin for Archaean banded iron formation-hosted gold deposits. Econ. Geol. 79, 162–171.

Pieczonka, J., Piestrzyński, A., Parańko, I., 2011. Geology of selected mineral deposit in Ukraine. Printed house – AGH-UST, pp. 157, (in Polish).

Pletnev, A.G., 1972. On the gold content of the iron-siliceous formation of the Likhman syncline of Krivoy Rog. Geol. J. 32 (2), 139–141 (in Russian).

Poorter, R.P.E., Varekamp, J.C., Poreda, R.J., Van Bergen, M.J., Krteulen, R., 1991. Chemical and isotopic composition of volcanic gases from the east Sinda and Banda areas, Indonedsia. Geochimia Cosmochimia Acta 55, 3795–3807.

Ribeiro-Rodrigues, L.C., Friedrich, G., Lobato, L.M., Duchini Jr., J., Vieira, F.W.V., 2000. Gold mineralization in the Quadrilátero Ferrífero, Minas Gerais, Brazil. In: Miller, H., Hervé, F. (eds.), Zeitschrift für Angewandte Geologie - Sonderheft, 1, 143–151.

Ridley, J.R., Diamond, L.W., 2000. Fluid chemistry of lode-gold deposits and implications for genetic models. In: Hagemann, S.G., Brown, P. (eds.), Gold in 2000. Reviews in Economic Geology. Society of Economic Geologists Inc. 13, pp. 141-162.

Robert, F., Poulsen, K.H., Cassidy, K.F., Hodgson, C.J., 2005. Gold Metallogeny of the Superior and Yilgarn Cratons, in Economic Geology 100th Anniversary Volume, 1001-1034.

Robert, F., Brommecker, R., Bourne, B.T., Dobak, P.J., McEwan, C.J., Rowe, R.R., Zhou, X., 2007. Models and Exploration Methods for Major Gold Deposit Types. p. In: Milkereit, B. (ed.), Proceedings of Exploration 07.Fifth Decennial International Conference on Mineral Exploration, 691-711.

Sakai, H., 1968. Isotopic properties of sulfur compounds in hydrothermal processes. Geochem. J. 2 (1), 29–49.

Sakai, H., Casadevall, T.J., Moore, J.G., 1982. Chemistry and isotope ratio of sulfur in basalts and volcanic gases at Kilauea volcano, Havaii. Geochim. Cosmochim. Acta 46, 2433–2441.

Schwartz, M.O., 2000. Cadmium in zinc deposits: economic geology of a polluting element. Int. Geol. Rev. 42 (5), 445–469.

Sharp, Z.D., Essene, E.J., Kelly, W.C., 1985. A re-examination of the arsenopyrite geothermometer: pressure considerations and applications to natural assemblages. Can. Mineral. 23, 517–534.

Simonson, B.M., 1985. Sedimentological constraints on the origins of Precambrian iron-formations. Geol. Soc. Am. Bull. 96 (2), 244. https://doi.org/10.1130/0016-7606(1985)96<244:SCOTOO>2.0.CO;2.

Sośnicka, M., Bakker, R.J., Broman, C., Pitcairn, I., Paranko, I., Burlinson, K., 2015. Fluid types and their genetic meaning for the BIF-hosted iron ores, Krivoy Rog, Ukraine. Ore Geol. Rev. 68, 171–194.

Sukach, V., Paranko, I., Kovalchuk, M., Yagovdik, O., Gayeva, N., 2013. Typomorphic features of native gold in hypergene alteration zone of ferruginous-siliceous rocks of the Kryvyi Rih structure (northern-tarapack ore occurrence). Mineral Rev. 63 (2), 76–82.

Sukach, V.V., Riazantseva, L.O., 2018. Complex Gold-Molybdenum deposits and occurrences in Greenstone Belts of the Middle Dnipro Region of the Ukrainian Shield. Mineralni Resursy Ukrainy 2. P., 3–9, (in Ukrainian).

Taylor, H.P., 1986. Magmatic volatiles: isotopic variation of C, H and S. Rev. Mineral 16, 185–225.

Tomkis, A.G., Frost, B.R., Pattison, D.R.M., 2006. Arsenopyrite melting during metamorphism of sulfide ore deposit. Canadian Mineral. 44, 1045–1062.

Velikanov, Y.V., Velikanova, O.Y, 2007. Orebearing zones of alkali metasomatism in the ferruginous-siliceous rocks of the Kryvbass. Collected papers "Shelochnoj magmatizm Zemli i ego rudonosnost". Doneck P., 25–28, (in Russian).

Velikanov, Y.F., Velikanova, O.Y., Nikolayenko, V.I., 2010. Ore mineralization of rock contact zone of of the Saksaganska and Gdantsevska Suites of the Kryvyi Rih series of the Kryvbass.Collected papers Institute of Environmental Geochemistry. Issue 18. Kyiv P., 173-180, (in Russian).

Vielreicher, R.M., Groves, D.I., Ridley, J.R., McNaughton, N.J., 1994. A replacement origin for the BIF-hosted gold deposit at Mt. Morgans, Yilgran Block, W.A. Ore Geology Reviews 9, Issue 4, 325-347. https://doi.org/10.1016/0169-1368(94)90003-5.

Woodall, R., 1979. Gold–Australia and the world. In: Glover, J. E., and Groves, D. I. (eds.), Gold mineralization: Nedlands, Univ. West-ern Australia, Geology Dept. Ext. Service Pub. 3, 1-34.

Yushin, A.A., Butyrin, V.K., 2009. Some problems of assessing the gold ore potential of Kryvyi Rih. Transactions of UkrNDMI NAN Ukraine 5 (part II), P., 336-343, (in Russian).

Yushin, A.A., Butyrin, V.K., Galchansky, L.V., Stadnishina, N.V., Bondarenko, I.N., 2008. Some geochemical features and prospects for identifying complex mineralization at the East Annovskoye deposit in Krivorozhye. Scientific works of Donetsk National Technical University. Mining and Geological Series. Issue 8 (136). P., 240-244, (in Russian).